

The Development of *N*- α -(2-Carboxyl)benzoyl-*N*⁵-(2-fluoro-1-iminoethyl)-L-ornithine Amide (*o*-F-amidine) and *N*- α -(2-Carboxyl)benzoyl-*N*⁵-(2-chloro-1-iminoethyl)-L-ornithine Amide (*o*-Cl-amidine) As Second Generation Protein Arginine Deiminase (PAD) Inhibitors[†]

Corey P. Causey,^{§,⊗} Justin E. Jones,^{‡,⊗} Jessica L. Slack,[‡] Daisuke Kamei,[⊥] Larry E. Jones, Jr.,[§] Venkataraman Subramanian,[‡] Bryan Knuckley,[‡] Pedram Ebrahimi,^{||} Alexander A. Chumanevich,^{||} Yuan Luo,[§] Hiroshi Hashimoto,[⊥] Mamoru Sato,[⊥] Lorne J. Hofseth,^{||} and Paul R. Thompson^{*,‡}

[†]Department of Chemistry, The Scripps Research Institute, 130 Scripps Way, Jupiter, Florida 33458, United States

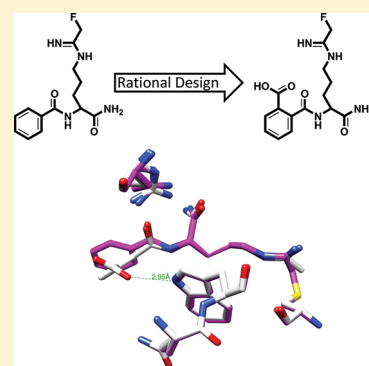
[§]Department of Chemistry & Biochemistry, University of South Carolina, 631 Sumter Street, Columbia, South Carolina 29208, United States

^{||}Department of Pharmaceutical and Biomedical Sciences, South Carolina College of Pharmacy, University of South Carolina, 770 Sumter Street, Columbia, South Carolina 29208, United States

[⊥]Graduate School of Integrated Science, Yokohama City University, 1-7-29 Suehiro-cho, Tsurumi-ku, Yokohama 230-0045, Japan

S Supporting Information

ABSTRACT: Protein arginine deiminase (PAD) activity is upregulated in a number of human diseases, including rheumatoid arthritis, ulcerative colitis, and cancer. These enzymes, there are five in humans (PADs 1–4 and 6), regulate gene transcription, cellular differentiation, and the innate immune response. Building on our successful generation of F- and Cl-amidine, which irreversibly inhibit all of the PADs, a structure–activity relationship was performed to develop second generation compounds with improved potency and selectivity. Incorporation of a carboxylate ortho to the backbone amide resulted in the identification of *N*- α -(2-carboxyl)benzoyl-*N*⁵-(2-fluoro-1-iminoethyl)-L-ornithine amide (*o*-F-amidine) and *N*- α -(2-carboxyl)benzoyl-*N*⁵-(2-chloro-1-iminoethyl)-L-ornithine amide (*o*-Cl-amidine), as PAD inactivators with improved potency (up to 65-fold) and selectivity (up to 25-fold). Relative to F- and Cl-amidine, the compounds also show enhanced potency in cellulose. As such, these compounds will be versatile chemical probes of PAD function.



INTRODUCTION

It has long been recognized that posttranslational modifications (PTMs) play critical roles in maintaining the homeostasis of biological systems. While many PTMs, and their putative roles in disease etiology, are well documented (e.g., protein phosphorylation), most others are less well understood. One example of the latter is protein deimination (Figure 1A).¹ This PTM is generated by the hydrolytic removal of ammonia from the guanidinium of a substrate arginine residue to generate a ureido group.^{1,2} Because this modification results in the formation of citrulline, this process is also termed citrullination. The enzymes responsible for generating this PTM are known as the protein arginine deiminases (PADs), and in humans and other mammals, there are five isozymes (i.e., PADs 1, 2, 3, 4, and 6) that possess a high degree of interisozyme sequence homology (~50%).^{1,3} Given that these isozymes possess similar, but not identical, substrate specificities,^{4,5} it is perhaps not surprising that the major distinguishing feature of individual family members is their tissue distribution patterns.³ For example, whereas PAD2 is near universally expressed

in all tissue and cell types, the expression patterns of the remaining PADs are much more restricted, with PADs 1, 3, 4, and 6 being most predominantly expressed in the skin, hair follicles, immune cells, and oocytes, respectively.³

Although one or more of these enzymes are expressed in virtually all cell types, our understanding of their physiological functions, especially with regard to PADs, 1, 2, 3, and 6, is limited. However, it is known that these enzymes play incompletely defined roles in a diverse number of processes, including the cornification of the skin (PADs 1, 2, and 3), hair follicle formation (PAD3), nerve myelination (PAD2), and fertility (PAD6).^{3,6–10} Given the early links suggesting that dysregulated PAD4 activity contributes to the onset and progression of rheumatoid arthritis (RA; see below and ref 1 for a review), our understanding of the physiological roles of PAD4, while still limited, is more advanced. For example, a fraction of PAD4 is localized to the nucleus where

Received: July 8, 2011

Published: September 01, 2011

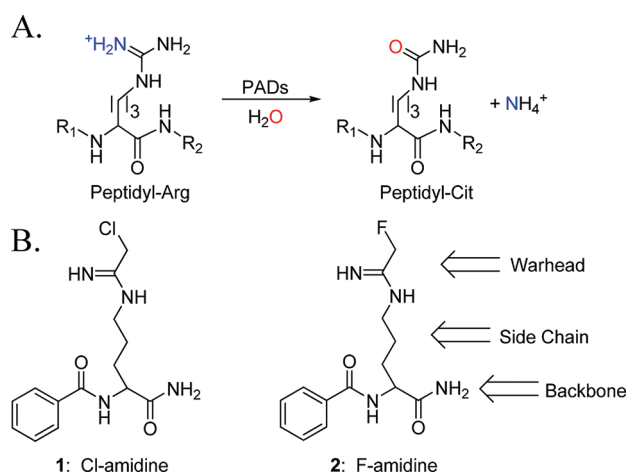


Figure 1. Protein arginine deiminase reaction and inhibitors. (A) The guanidinium group of an arginine residue is converted into a ureido group to form citrulline. (B) Structures of Cl- and F-amidine.

it has been shown to modify the unstructured tails of histones H3 and H4, and this modification has been associated with the decreased transcription of genes under the control of a number of transcription factors, including the estrogen receptor, thyroid receptor, and p53.^{11–14} More recently, PAD4 was shown to deiminate ELK1, and this PTM was associated with increased transcription of the proto-oncogene *c-Fos*.¹⁵

In addition to modulating gene transcription, PAD4 activity has been shown to affect a variety of processes, including apoptosis (inhibition and overexpression of PAD4 induces apoptosis)^{13,14,16} and differentiation (PAD4 inhibition triggers the differentiation of HL60 cells into HL60 granulocytes and monocytes).¹⁷ Emerging evidence also suggests that PAD4 may play a key role in regulating at least a subset of the innate immune response. For example, PAD4 has been shown to deiminate a number of chemokines (e.g., CXCL 5, 8, 10, 11, and 12), and this modification reduces their ability to trigger chemotaxis and cell signaling *in vitro*.^{18–20} Additionally, PAD4 activity appears to be critical for the formation of Neutrophil Extracellular Traps (NETs), as Cl-amidine (Figure 1B), a pan-PAD inhibitor developed by our lab,²¹ prevents NET formation;^{22,23} neutrophils extravate their chromatin to form net-like structures in response to a number of signaling molecules of both bacterial (e.g., LPS and fMLP)^{22–24} and human origin (e.g., CXCL2 and CXCL8).²⁵

Dysregulated PAD expression and activity has been associated with a number of human diseases, including rheumatoid arthritis (RA), ulcerative colitis, Crohn's disease, glaucoma, multiple sclerosis, Alzheimer's disease, and even cancer (for a review, see ref 1). Although the association between dysregulated PAD activity and human disease seems clear, especially with our recent demonstration that Cl-amidine decreases disease severity in the collagen induced arthritis (CIA) model of RA and the dextran sodium sulfate (DSS) model of ulcerative colitis,^{26,27} what is not known are the specific identities of the isozymes involved in the onset and progression of these pathologies. From the available evidence, the most likely candidates appear to be PADs 2 and 4, as these enzymes are expressed by immune cells (the diseases listed above all have an autoimmune component), and both are overexpressed in these diseases.^{1,3,28,29} With respect to RA, the evidence linking dysregulated PAD4 activity to the onset and progression of this disease are particularly strong. For example,

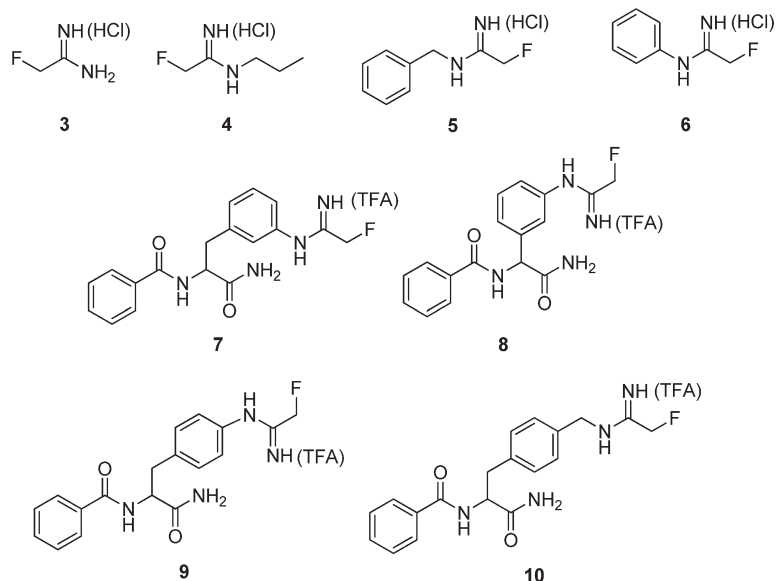
patients with RA produce autoantibodies targeting both citrullinated proteins and PAD4 itself, and these autoantibodies first appear in the preclinical phase of the disease.^{30–33} Additionally, mutations in the gene encoding PAD4 confer an increased risk of developing RA, at least in Asian populations.^{34,35} Finally, PAD4 and citrullinated proteins are present in the inflamed joints of RA patients.^{28,36} However, the fact that PAD2 is also overexpressed in these tissues²⁸ complicates the seemingly simple picture that dysregulated PAD4 activity is the only PAD that contributes to the etiology of RA. Thus, it is unclear whether the inhibition of single or multiple PADs is required to treat these diseases. One way to address this issue is the development of isozyme-specific PAD inhibitors that can be used to discern the relative contributions of individual PADs to human disease. To begin to develop such compounds and also identify compounds with enhanced potency and bioavailability, we performed Structure–Activity Relationships (SARs) on our previously described PAD inhibitors F- and Cl-amidine (Figure 1B). Herein we describe the design, synthesis, and testing of a series of new PAD inhibitors with enhanced potency, selectivity, and bioavailability. In particular, we describe the development of *o*-F-amidine and *o*-Cl-amidine as two of the most potent and partially selective PAD inhibitors described to date.

RESULTS AND DISCUSSION

Design, Synthesis, and Characterization of X-Amidine Side Chain Analogs. The structure of F-amidine, which is used as a baseline for comparison, can be divided into three main portions: the warhead, the side chain, and the backbone (Figure 1B). To better understand the relative contribution of the side chain to inhibitor potency, we initially synthesized 2-fluoro-*N*-propylacetamidine (4) (Figure 2), which is essentially a propylamine modified warhead, to mimic the three-carbon side chain portion of F-amidine. The compound was synthesized by reaction of propylamine with 2-fluorothioacetimidate and purified, and IC₅₀ values were obtained for PAD4. The results indicate that 4 is a relatively weak PAD4 inhibitor (IC₅₀ > 1 mM; Table 2) and that the IC₅₀ value is comparable to that obtained for the warhead alone, i.e., 3. The fact that F-amidine is approximately 2 orders of magnitude more potent than 4 indicates that the side chain component of F-amidine is not responsible for the relatively high potency of F-amidine.

Given that a tryptophan residue (i.e., W347) lines the active site of PAD4 and interacts with the side chain portion of F-amidine via hydrophobic and van der Waals interactions (Figure 3), we considered the possibility that the incorporation of an aromatic moiety, in place of the aliphatic side chain, would interact favorably with the W347 indole group. To test this hypothesis, the fluoroacetamidine warhead was installed on two structurally similar aromatic amines, i.e., aniline and benzylamine. However, neither the benzyl (5: IC₅₀ > 1 mM) nor the aniline (6: IC₅₀ > 500 μM) derivatives were potent PAD4 inhibitors. Nevertheless, the fact that the aniline derivative was more potent than the baseline compound, i.e., the propyl derivative, suggested that its incorporation into the full inhibitor might enhance inhibitor potency. To examine this possibility, we synthesized and compared the relative potencies of phenylalanine and phenylglycine derivatives in which the warhead is placed meta to the α-carbon. Note that both the phenylalanine and phenylglycine derivatives were synthesized to explore how differences in the connectivity to the backbone affect inhibitor potency. The results of these

A. Side Chain Substitutions



B. Backbone Substitutions

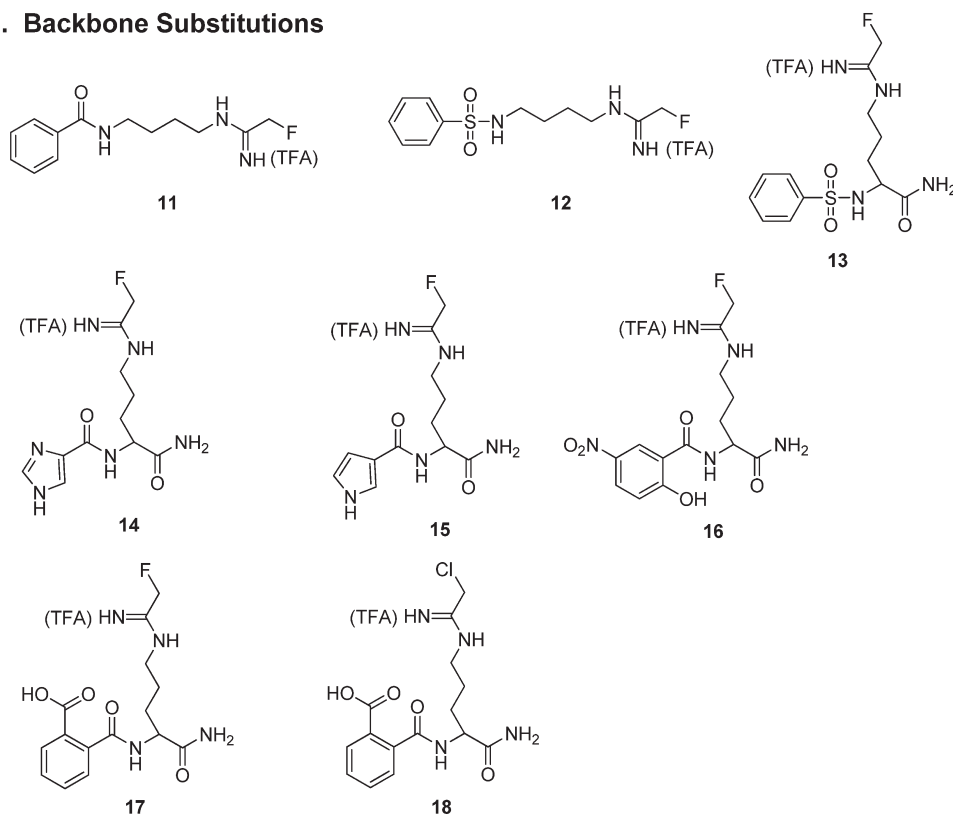


Figure 2. Structures of side chain analogues (A) and backbone analogues (B).

SAR studies indicated that the phenylalanine derivative, i.e., **7** ($IC_{50} = \sim 300 \mu M$), was more potent than the phenylglycine derivative (**8**) ($> 2 \text{ mM}$) suggesting that the extra methylene unit between the backbone and warhead is advantageous. Given that these values are significantly less than those obtained with F-amidine and represent only a slight improvement over the aniline derivative on its own, we considered the possibility that the lack of potency was due to a less than ideal positioning of the warhead about the phenyl ring. To partially test this hypothesis,

two para-substituted phenylalanine derivatives, i.e., compounds **9** and **10**, were synthesized. The first compound attaches the warhead directly to the phenyl ring, mimicking the structure of the aniline, and the second compound attaches the warhead via a one carbon methylene linker that was expected to project the warhead further into the active site where it might react more favorably with the enzyme. Unfortunately, the IC_{50} values obtained for compounds **9** and **10** ($IC_{50} \sim 300 \mu M$ and $> 1 \text{ mM}$, respectively) are similar to those determined for the ortho-substituted derivatives,

Table 1. Crystallographic Data and Refinement Statistics^a

inhibitor	<i>o</i> -F-AM	<i>o</i> -Cl-AM
soaking	5 mM, 6 h	5 mM, 6 h
crystallographic data		
space group	C2	C2
cell dimensions	$a = 146.4, b = 60.4,$ $c = 115.5 \text{ \AA}$	$a = 145.7, b = 60.8,$ $c = 114.3 \text{ \AA}$
	$\beta = 124.4^\circ$	$\beta = 123.9^\circ$
resolution range (\AA)	50.0–2.1 (2.18–2.10)	50.0–2.5 (2.59–2.50)
total observations	155,187	98,188
unique observations	44,771	27,393
completeness (%)	91.8 (66.7)	94.8
R_{merge} (%)	4.5 (28.8)	6.2 (40.1)
$\langle I \rangle / \sigma \langle I \rangle$	14.9	14.8
refinement statistics		
resolution (\AA)	20.0–2.1	20.0–2.5
R/R_{free} (%)	22.0/25.0	20.3/24.4
root mean square deviation		
bond lengths (\AA)	0.005	0.009
bond angles (deg)	0.887	1.241

^a Values in parentheses are for the highest resolution shell.

Table 2. IC₅₀ Values of PAD4 Inhibitors^a

compd	IC ₅₀
1	5.9 ± 0.3 μM
2	22 ± 2.1 μM
3	>10 mM
4	>1 mM
5	>1 mM
6	>0.5 mM
7	310 ± 37 μM
8	2.1 ± 0.3 mM
9	310 ± 110 μM
10	>1 mM
11	>1 mM
12	>1 mM
13	500 ± 60 μM
14	230 ± 110 μM
15	19 ± 3.0 μM
16	12 ± 6.4 μM
17	1.9 ± 0.2 μM
18	2.2 ± 0.3 μM

^a Given that these compounds are time dependent irreversible inactivators, these IC₅₀ values should be considered apparent measures of affinity.

thereby indicating that the replacement of the aliphatic side chain of F-amidine with a phenyl moiety does not lead to inhibitors with enhanced potency.

Design, Synthesis, and Characterization of X-Amidine Backbone Analogues. Since none of the side chain analogues were more potent than F-amidine, we considered whether changes to the backbone might yield inhibitors with enhanced potency. The backbone component of F-amidine contains two amide bonds that are presumed, although not yet proven, to be important for binding to the enzyme. To determine whether this was indeed

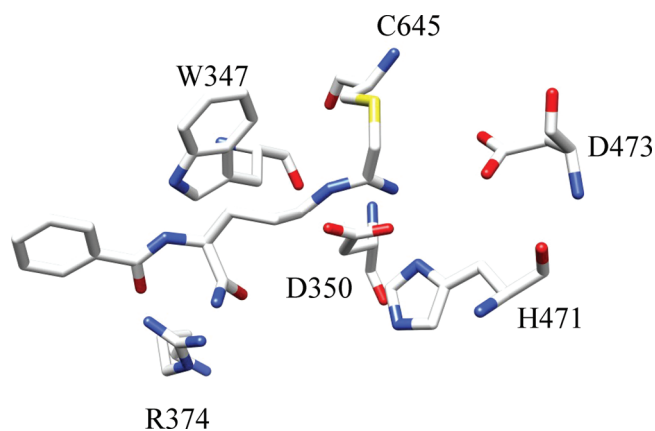


Figure 3. Crystal structure of PAD4·F-amidine complex. This figure was prepared with UCSF Chimera using the coordinates for the PAD4·F-amidine complex (PDB ID: 2DW5).

the case, we synthesized compound **11** (Figure 2B), which lacks the C-terminal carboxamide moiety. The IC₅₀ value obtained for this compound (IC₅₀ ≥ 500 μM) confirms that both amide groups are critical for the overall potency of F-amidine. We next considered the effect of substituting the benzoyl-carboxamide for a sulfonamide (**12**). While this substitution retains the H-bond acceptor and in fact introduces a second one, the spatial orientation is somewhat different; the sulfonamide has a tetrahedral geometry, while the carboxamide has a trigonal planar geometry. Although it was impossible to predict exactly how this substitution would affect the potency, the experimental evidence (IC₅₀ > 1 mM) clearly indicates that the effect was deleterious. To determine whether the lack of potency was solely due to the loss of the C-terminal carboxamide, the introduction of the sulphonamide, or a combination of both changes, we next synthesized compound **13**, which retains the C-terminal carboxamide but replaces the benzoyl-carboxamide with a sulfonamide. Interestingly, this compound was also a poor PAD4 inhibitor, which, combined with the results described above for compounds **11** and **12**, suggests that hydrogen bonding between R374 and the two backbone carbonyls contributes to the potency of F-amidine in a synergistic fashion.

Given that substitutions altering the two backbone carbonyls, as well as the side chain, yielded inhibitors with decreased potency, we considered that substitutions of the benzoyl group might yield inhibitors with increased potency. In particular, we considered substitutions that would mimic an extension of the peptide chain. Our first attempt replaced the phenyl ring with an imidazole ring (**14**). This substitution maintains the aromatic character of the phenyl ring while incorporating an NH moiety that might mimic a peptide NH, thus becoming a hydrogen bond donor; an additional hydrogen bond could significantly increase the binding affinity of the inhibitor. The results of inhibition studies with **14** showed a 10-fold decrease in potency relative to F-amidine (IC₅₀ = 230 ± 110 μM). This result was somewhat unexpected given that even in the absence of an additional H-bond, the imidazole moiety was still aromatic and thus should be, at worst, comparable to the phenyl moiety. Upon further consideration, however, we realized that the imidazole was likely protonated under the reaction conditions resulting in a positively charged species. Therefore, we concluded that the decrease in potency may actually arise from a charge–charge repulsion between

Table 3. Inhibition of PAD Isozymes by Haloacetamidine-Based Inhibitors

compd	isozyme	IC ₅₀ ^a (μM)	k _{inact} (min ⁻¹)	K _I (μM)	k _{inact} /K _I (M ⁻¹ min ⁻¹)
F-amidine	PAD1	29 ± 1.32	0.30 ± 0.03	110 ± 40	2800
	PAD2	51 ± 8.96	ND ^b	ND ^b	380
	PAD3	367 ± 189	0.05 ± 0.01	293 ± 193	170
	PAD4	22 ± 2.10	1.0 ± 0.1	330 ± 90	3000
Cl-amidine	PAD1	0.8 ± 0.3	2.3 ± 0.1	62 ± 11	37000
	PAD2	17 ± 3.1	ND ^b	ND ^b	1200
	PAD3	6 ± 1.0	0.056 ± 0.005	28 ± 7.3	2000
	PAD4	5.9 ± 0.3	2.4 ± 0.2	180 ± 33	13000
<i>o</i> -F-amidine	PAD1	1.4 ± 0.41	1.7 ± 0.1	9.4 ± 1.8	180900
	PAD2	≥ 50	ND ^b	ND ^b	7500
	PAD3	34 ± 31.9	ND ^b	ND ^b	6700
	PAD4	1.9 ± 0.21	0.5 ± 0.17	16 ± 9	32500
<i>o</i> -Cl-amidine	PAD1	0.84 ± 0.12	ND ^a	ND ^a	106400
	PAD2	6.2 ± 0.7	ND ^a	ND ^a	14100
	PAD3	0.69 ± 0.34	0.3 ± 0.06	29 ± 12	10345
	PAD4	2.2 ± 0.31	0.5 ± 0.11	13 ± 5.2	38000

^a Given that these compounds are time dependent irreversible inactivators, these IC₅₀ values should be considered apparent measures of affinity. ^b ND = Not determinable. Values for k_{inact} and K_I could not be determined because saturation was not observed in the plots of k_{obs} versus inactivator concentration. k_{inact}/K_I values were determined from linear fits of the data.

the protonated imidazole and a positively charged residue on the enzyme.

In order to circumvent this potential charge–charge repulsion, we chose to substitute the phenyl ring with a pyrrolidine ring (**15**). This substitution maintains both the aromaticity and the NH bond as a potential H-bond donor, but given the much higher pK_a, the pyrrolidine remains neutral under the assay conditions. Synthesis and evaluation of this derivative was carried out, and the results indicate a potency that is comparable to that of F-amidine. Although this inhibitor is not more potent than the parent compound, the fact that the IC₅₀ is the same as the benzoylated version suggests two things: (i) the NH may contribute little to overall binding; and (ii) the loss of potency seen with the imidazole derivative is likely due to a charge–charge repulsion.

Because the results from the imidazole and pyrrolidine derivatives suggest the presence of a positively charged residue in close proximity to the active site, we postulated that the incorporation of a negatively charged moiety on the benzoyl group would increase inhibitor potency. Toward this end, we chose to substitute the phenyl ring of F-amidine with a *para*-nitro-phenol (**16**). We postulated that the positioning of the nitro group *para* to the hydroxyl would sufficiently depress the pK_a of the hydroxyl to generate an inhibitor that is at least partially deprotonated. This negative charge should then be positioned to interact with the positively charged residue on the enzyme without being sterically cumbersome. Once this derivative was synthesized and tested, the results showed a small decrease (~2-fold) in potency (IC₅₀ = 12.1 ± 6.4 μM).

Given these promising results, we next designed and synthesized an F-amidine derivative that incorporated a carboxylate ortho to the backbone amide (**17**). Synthesis of this derivative, which is denoted *o*-F-amidine, was accomplished by using phthalic anhydride in the place of benzoyl chloride. As predicted, the IC₅₀ of this compound (1.9 ± 0.21 μM) is 10-fold lower than that obtained with the parent compound, F-amidine. Given that the substitution of chloride for fluoride typically increases the potency of X-amidine inhibitors by ~5-fold, we anticipated a similar trend in these derivatives as well. However, once the

chloride derivative was synthesized and assayed, we found that the inhibitory potency of *o*-Cl-amidine (**18**) (IC₅₀ = 2.2 ± 0.31 μM) was nearly identical to that of *o*-F-amidine.

Mechanism of Inhibition. Since the parent compounds, i.e., F- and Cl-amidine, are mechanism based inactivators, we next determined whether *o*-F- and *o*-Cl-amidine also irreversibly inactivate PADs 1, 2, 3, and 4. For these studies, a preformed complex of inactivator and enzyme was generated, then dialyzed for 20 h, at which point the residual activity was measured. As shown in Figure S1 of the Supporting Information, little to no recovery of activity was observed for all of the PADs tested, thereby confirming that, like F- and Cl-amidine, *o*-F- and *o*-Cl-amidine are irreversible PAD inactivators. In order to help confirm that PAD inactivation is due to the modification of an active site residue, substrate protection experiments were performed. For these studies, product formation was measured as a function of time at 2 different concentrations of substrate (10 and 2 mM benzoyl-L-arginine ethyl ester (BAEE)) with and without inactivator. The results (Figure S2 in the Supporting Information) indicate that for PADs 1, 2, 3, and 4 the rates of inactivation are slower at higher substrate concentrations. Such a result is most consistent with enzyme inactivation being due to the modification of an active site residue, which, based on precedence, is likely the active site cysteine.

Selectivity Studies. To evaluate the selectivity of *o*-F- and *o*-Cl-amidine, k_{inact}, K_I, and k_{inact}/K_I values were determined for all of the PADs (Table 3). Note that for irreversible inhibitors these rate constants provide a more accurate assessment of selectivity than IC₅₀ values. For these experiments, the residual activity was measured as a function of time with increasing concentrations of inactivator (see Figure 4A,C for representative data). From these curves, the pseudo-first order rate constants of inactivation (i.e., k_{obs}) were determined and plotted against inactivator concentration and fit to eq 4 to provide values for k_{inact}, K_I, and k_{inact}/K_I (see Figure 4B,D for representative data). Interestingly, based on the k_{inact}/K_I values, *o*-Cl-amidine preferentially inactivates PAD1, as the k_{inact}/K_I value obtained for this isozyme is 8-, 10-,

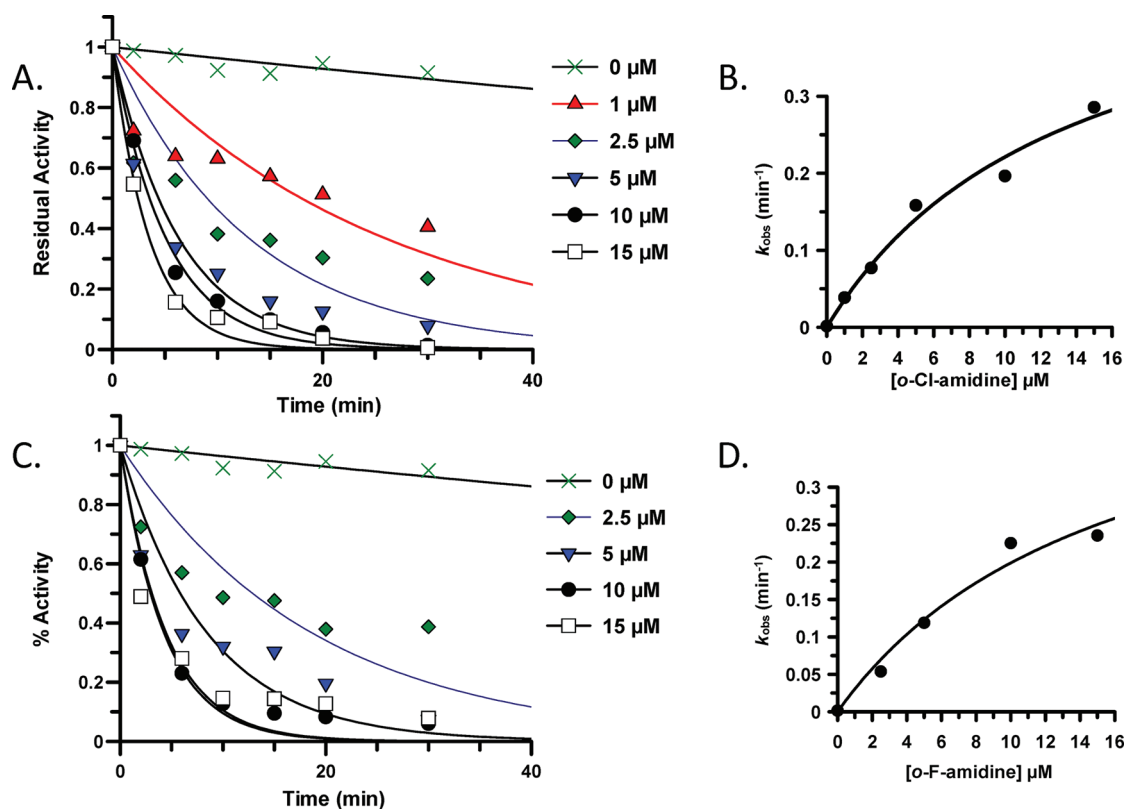


Figure 4. Inactivation of PAD4 with *o*-F- and *o*-Cl-amidine. The residual activity of PAD4 was measured versus time with increasing concentrations of (A) *o*-F-amidine and (C) *o*-Cl-amidine. The rates (k_{obs}) were plotted versus the concentration of (B) *o*-F-amidine and (D) *o*-Cl-amidine to obtain the inactivation parameters.

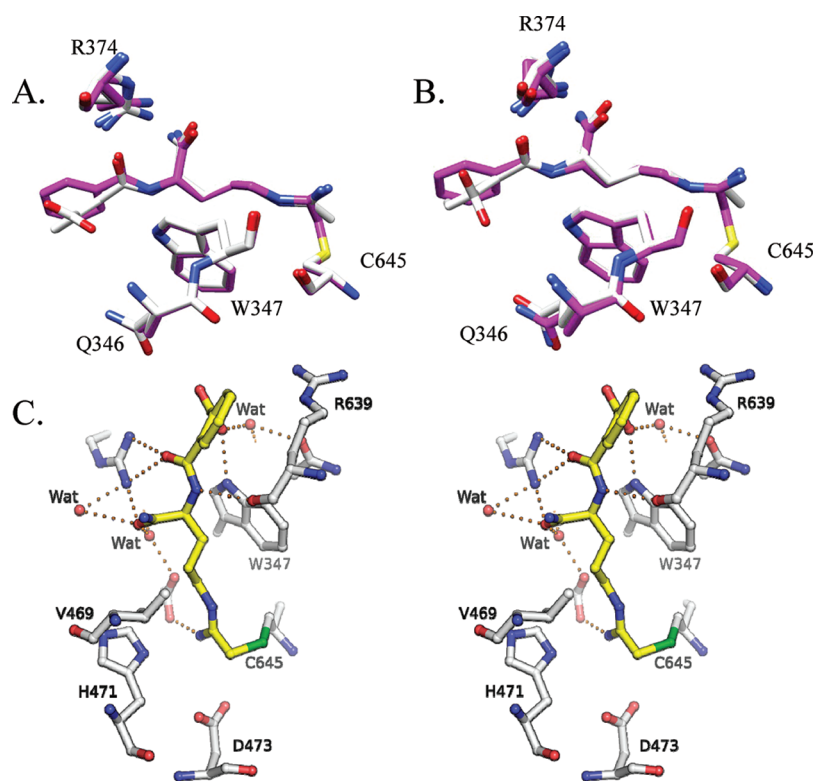


Figure 5. Overlays of the crystal structure of PAD4 with (A) F-amidine and *o*-F-amidine bound and (B) Cl-amidine and *o*-Cl-amidine bound. (C) Stereoview of the crystal structure of PAD4 bound to *o*-F-amidine.

3-fold higher than that obtained for PADs 2, 3, and 4, respectively. Similar trends were observed for *o*-F-amidine, where the k_{inact}/K_i values are 24-, 27-, and 6-fold higher for PAD1 than for PADs 2, 3, and 4, respectively. Given that the relative selectivity of *o*-Cl-amidine for PADs 1 and 4 is relatively modest (~ 3 -fold), this compound is a PAD1 and 4 selective inhibitor, whereas *o*-F-amidine is primarily a PAD1 selective inhibitor. It is also important to note that *o*-F-amidine is 60-fold more potent than the parent compound F-amidine.

Structural Studies. To help determine the molecular basis for the enhanced potency of both *o*-F- and *o*-Cl-amidine, the structures of these compounds bound to the PAD4·calcium complex were determined and compared to the structure of PAD4·calcium·F-amidine (Figure 5A,B). The structures of these complexes are virtually superimposable (rmsd = 0.222 Å for comparable 573 C α) and revealed the presence of three potential residues, i.e., Q346, W347, and R374, that could provide favorable hydrogen bonding and/or electrostatic interactions with the *ortho*-carboxylate that would explain the enhanced potency of *o*-F- and *o*-Cl-amidine (Figure 5C). While the distance between the indole NH of W347 and the *ortho*-carboxylate is characteristic of a hydrogen bond (i.e., 2.9 Å), the distances between the *ortho*-carboxylate and the carboxamide of Q346 (i.e., 3.9 Å) and the guanidinium group of R374 (i.e., 4.6–5.6 Å) are greater than that typically associated with such an interaction. Note that in the *o*-F-amidine complex, water-mediated hydrogen bonds between Q347 and the carboxylate of *o*-F-amidine are observed because of higher-resolution data. Given that these structures represent the dead-end complex and as such do not represent the initial encounter

complex where the effects of the *ortho*-carboxylate on enzyme inactivation are expected to be most profound, we used site directed mutagenesis to identify the residue(s) that is/are most critical for inhibitor recognition. Specifically, Q346, W347, and R374 were individually converted to alanine, and IC₅₀ values were determined for the mutant enzymes. To aid our analysis, we also generated the Q346E, W347F, and R374K mutants. The results of these studies (Table 4) indicate that mutation of Q346 to either an alanine or a glutamate had essentially no effect on the IC₅₀ values determined for *o*-F- and *o*-Cl-amidine, suggesting that the enhanced potency of these compounds is not due to an interaction between the carboxylate and carboxamide moieties on the inhibitor and Q346, respectively. In contrast, the IC₅₀ values determined for the R374K and R374A mutants are ~ 2.4 -fold and 28-fold higher for *o*-F-amidine when compared to the values obtained for the wild-type enzyme. Since similar effects on potency were observed for F-amidine, these results suggest that the interaction between the *ortho*-carboxylate and the R374 guanidinium is not crucial for the enhanced potency of these PAD inactivators. Nevertheless, this arginine residue is conserved in both PADs 1 and 4, and the presence of R374 may explain why *o*-F- and *o*-Cl-amidine preferentially inactivate these enzymes. Unfortunately, neither of the tryptophan mutants were active ($k_{\text{cat}}/K_m \leq 0.2 \text{ M}^{-1} \text{ s}^{-1}$); thus, the importance of the indole NH group to inhibitor potency could not be evaluated directly. Nevertheless, this interaction is likely important when one considers the fact that the introduction of the *ortho*-carboxylate led to enhanced potency among all the isozymes and the fact that this residue is universally conserved among the PAD isozymes.

Bioavailability of *o*-F- and *o*-Cl-Amidine. To illustrate the utility of *o*-F- and *o*-Cl-amidine as chemical probes of in vivo PAD4 function, we set out to evaluate their activity in cellulose. Initially, the bioavailability of the compounds was determined by monitoring their effects on histone H3 citrullination in HL60 granulocytes; PAD4 is known to deiminate histone H3 in this cell line in response to the calcium ionophore A23187.^{37,38} Western blots, using an anticitrullinated histone H3 antibody, demonstrated that the levels of deiminated histone H3 are decreased upon a 30 min incubation with the inhibitors. Significantly, the improved in vitro potency of *o*-F- and *o*-Cl-amidine is paralleled in cellulose, as exemplified by the fact that as little as 1 μM of

Table 4. PAD4 IC₅₀ Values

enzyme	IC ₅₀		IC ₅₀	
	<i>o</i> -F-amidine (μM)	<i>o</i> -Cl-amidine (μM)	F-amidine (μM)	Cl-amidine (μM)
wild-type	1.9 \pm 0.21	2.2 \pm 0.31	22 \pm 2.1	5.9 \pm 0.3
Q346E	1.1 \pm 0.31	2.4 \pm 0.17	21 \pm 2.2	4.0 \pm 1.6
Q346A	0.4 \pm 0.02	1.1 \pm 0.19	51 \pm 2.6	3.4 \pm 0.8
R374K	4.6 \pm 2.79	5.3 \pm 0.54	15 \pm 5.5	9.0 \pm 1.6
R374A	32 \pm 11	22 \pm 0.75	530 \pm 42	15 \pm 4.0

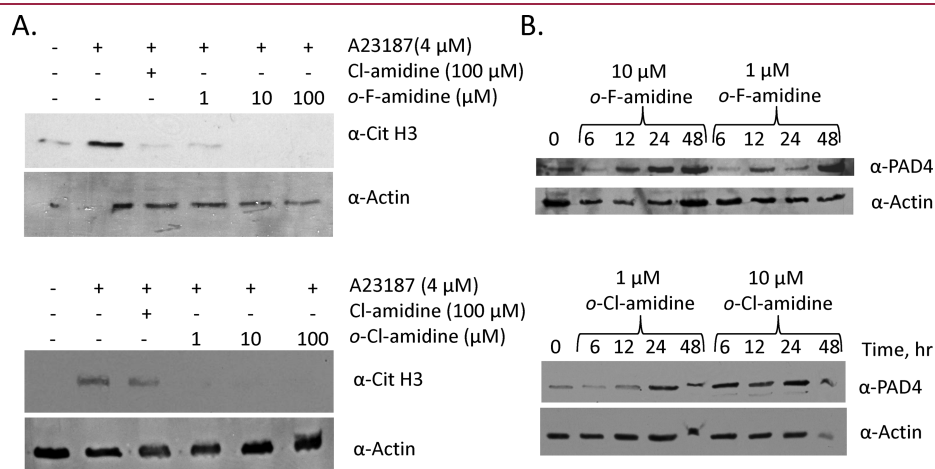


Figure 6. (A) Levels of citrullinated histone H3 in HL-60 granulocytes after treatment with *o*-F- and *o*-Cl-amidine. (B) *o*-F- and *o*-Cl-amidine induce the differentiation of HL-60 cells. HL-60 cells were exposed to either *o*-F- or *o*-Cl-amidine over the course of 48 h with time points taken after 6, 12, 24, and 48 h.

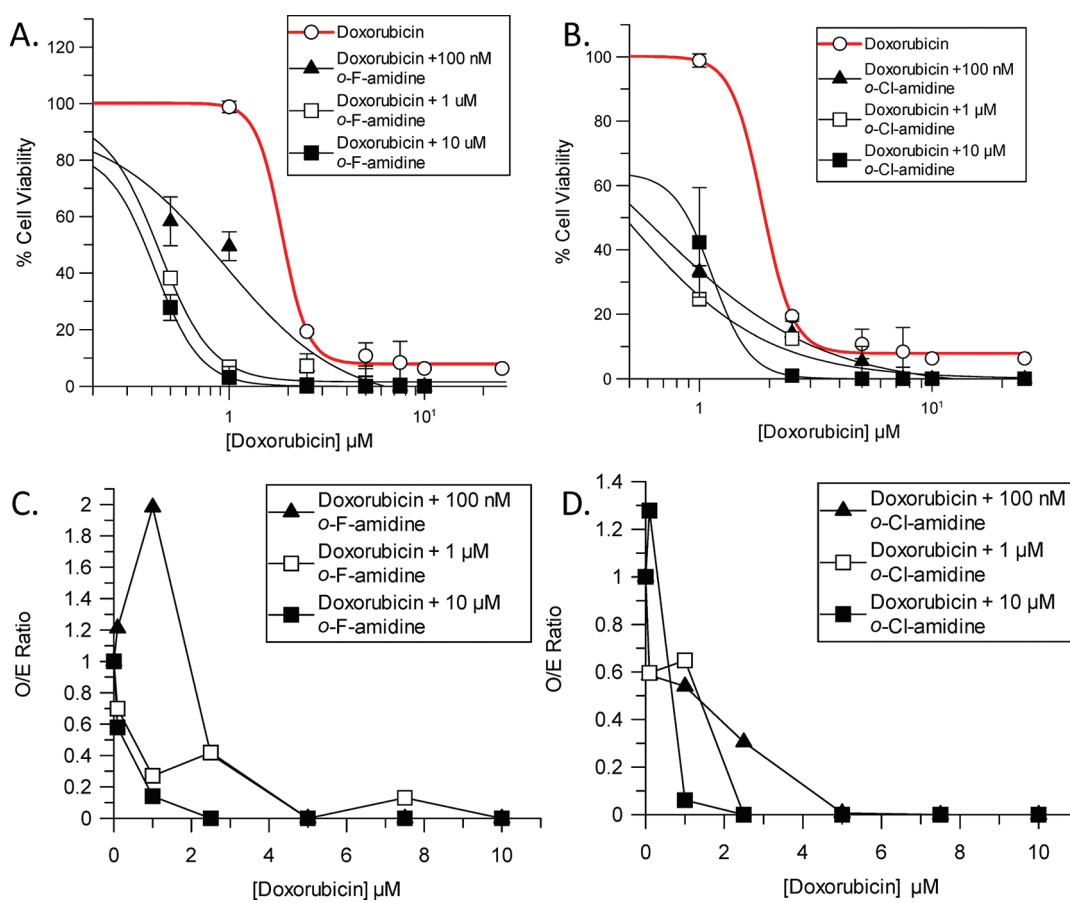


Figure 7. Effects of *o*-F-amidine (A) and *o*-Cl-amidine (B) in combination with doxorubicin on cell viability of HL-60 cells. Cell viability was measured, using a standard MTT assay, after a 24 h incubation with the inhibitors. Each data point represents an average of three trials ($p < 0.05$). The combination of *o*-F-amidine (C) and *o*-Cl-amidine (D) with doxorubicin resulted in synergistic killing of HL-60 cells. Synergistic, additive, and subadditive effects of the combination therapy were determined by a comparison of the O/E ratios, where $O/E < 0.8$ is considered synergistic, $O/E = 0.8–1.2$ is additive, and an $O/E > 1.2$ is subadditive.

o-F-amidine decreased the levels of deiminated histone H3 to the same extent as 100 μM of Cl-amidine (Figure 6A).

Effect of *o*-F- and *o*-Cl-Amidine on Cell Viability. Having demonstrated that the additional carboxylate does not affect the bioavailability of these inhibitors, we next investigated whether these compounds potentiate the cell killing effects of doxorubicin, similarly to the parent compounds F- and Cl-amidine.¹⁷ For these experiments, the effect of doxorubicin on HL-60 cell survival was determined in the absence and presence of increasing concentrations of *o*-F- and *o*-Cl-amidine using the standard MTT assay. As depicted in Figure 7, addition of *o*-F- and *o*-Cl-amidine caused the dose–response curves to shift to the left, resulting in an approximate 6-fold decrease in the EC_{50} for doxorubicin (Table 5). The fact that the magnitude of the effect is similar for both *o*-F- and *o*-Cl-amidine is consistent with the fact that these compounds are equipotent PAD4 inhibitors. Relative to 1 μM Cl-amidine, which reduced the EC_{50} by ~ 2 -fold, both *o*-F- and *o*-Cl-amidine decreased the EC_{50} by ~ 6 -fold at concentrations as low as 100 nM. In addition to decreasing the EC_{50} of doxorubicin, both compounds also decrease cell survival to background levels, i.e., no viable cells were detectable. To determine whether the effects imparted by *o*-F- and *o*-Cl-amidine on doxorubicin cell cytotoxicity were subadditive, additive, or synergistic, the additive model was used.^{39,40} This model predicts that two drugs are subadditive when the observed/expected

Table 5. Cytotoxicity of *o*-F- and *o*-Cl-amidine in Combination with Doxorubicin in HL-60 Cells^a

conditions	EC_{50} (μM)	% survival
doxorubicin	2.50 ± 1.16	12.0 ± 4.4
doxorubicin + 100 nM <i>o</i> -Cl-amidine	0.39 ± 0.02	ND ^b
doxorubicin + 1 μM <i>o</i> -Cl-amidine	0.34 ± 0.03	ND ^b
doxorubicin + 10 μM <i>o</i> -Cl-amidine	0.34 ± 0.12	ND ^b
doxorubicin + 100 nM <i>o</i> -F-amidine	0.45 ± 0.12	ND ^b
doxorubicin + 1 μM <i>o</i> -F-amidine	0.44 ± 0.03	ND ^b
doxorubicin + 10 μM <i>o</i> -F-amidine	0.42 ± 0.01	ND ^b
doxorubicin + 1 μM Cl-amidine	1.42 ± 0.02	ND ^b
doxorubicin + 10 μM Cl-amidine	1.29 ± 0.04	ND ^b
doxorubicin + 100 μM Cl-amidine	0.14 ± 0.09	ND ^b
doxorubicin + 1 μM F-amidine	2.33 ± 1.74	8.14 ± 5.10
doxorubicin + 10 μM F-amidine	1.30 ± 0.66	ND ^b
doxorubicin + 100 μM F-amidine	0.49 ± 0.25	ND ^b

^a EC_{50} is defined as the concentration of agent that reduces cell viability to 50% of maximum. EC_{50} values were determined by fitting the dose–response data to eq 1. % survival is based on the cell viability at the maximum agent concentration tested. ^b ND: no viable cells were detected as defined by the lack of absorbance above the 100% killing control.

(O/E) ratio is 1.2, additive when the O/E ratio is between 0.8 and 1.2, and synergistic when the O/E ratio is <0.8 . As depicted in Figure 7C,D, *o*-F- and *o*-Cl-amidine potentiate the cell killing of doxorubicin in HL-60 cells in a synergistic and dose dependent fashion.

***o*-F- and *o*-Cl-Amidine Mediated Differentiation of HL60 Cells.** Given that F- and Cl-amidine can trigger the differentiation of multiple cancer cell lines,¹⁷ including the differentiation of HL60 cells into HL60 granulocytes, we evaluated whether *o*-F- and *o*-Cl-amidine can also act as differentiating agents. For these experiments, PAD4 expression levels were monitored after the treatment of HL60 cells with *o*-F- and *o*-Cl-amidine; PAD4 expression levels are increased upon the differentiation of HL60 cells. Western blots, using an anti-PAD4 antibody, indicate that *o*-F- and *o*-Cl-amidine treatment causes a dose and time dependent increase in PAD4 protein expression. For example, at the highest doses of *o*-F- and *o*-Cl-amidine tested (i.e., 10 μ M), PAD4 expression was apparent after only 6 h of treatment; however, with lower doses (e.g., 1 μ M), increased levels of this enzyme were observed only after 12 and 24 h. In total, the results of these experiments demonstrate that these inhibitors differentiate HL-60 cells into HL-60 granulocytes in a manner similar to that of the parent compounds.

Inflammatory Cell Apoptosis. We have recently shown that Cl-amidine induces inflammatory cell apoptosis in vitro and in vivo²⁷ and have suggested that this inhibitor may suppress

colitis by removing the cells that drive colitis. With the increased potency of *o*-F-amidine, we thought it would be prudent to test the hypothesis that *o*-F-amidine has a more potent impact on inflammatory cell apoptosis than Cl-amidine. Results shown in Figure 8 are consistent with this hypothesis. For example, representative scatterplots of Annexin V/propidium iodide staining following the exposure of TK6 lymphoblastoid cells to *o*-F-amidine (50 μ M) or Cl-amidine (50 μ M) for up to 8 h demonstrate that *o*-F-amidine increases the number of apoptotic cells to a greater extent than an equivalent concentration of Cl-amidine (Figure 8A). Figure 8B depicts the quantification of apoptosis (4th quadrant). Additionally, *o*-F-amidine induces PARP cleavage earlier and to a greater extent than the same concentration of Cl-amidine (Figure 8C).

CONCLUSIONS

In conclusion, SAR led to the development of two new PAD inhibitors, *o*-F- and *o*-Cl-amidine, that are significantly (up to 65-fold) more potent than F- and Cl-amidine. The increased potency is due to the carboxylate functionality in the ortho position of the benzoyl ring. Although the inclusion of this group enhanced potency for all of the PADs, the effects are isozyme and warhead dependent. For example, with *o*-Cl-amidine, the increase in $k_{\text{inact}}/K_{\text{I}}$ ranged from 3-fold for PADs 1 and 4 to 12-fold for PAD2, whereas for *o*-F-amidine, the $k_{\text{inact}}/K_{\text{I}}$ values were increased by

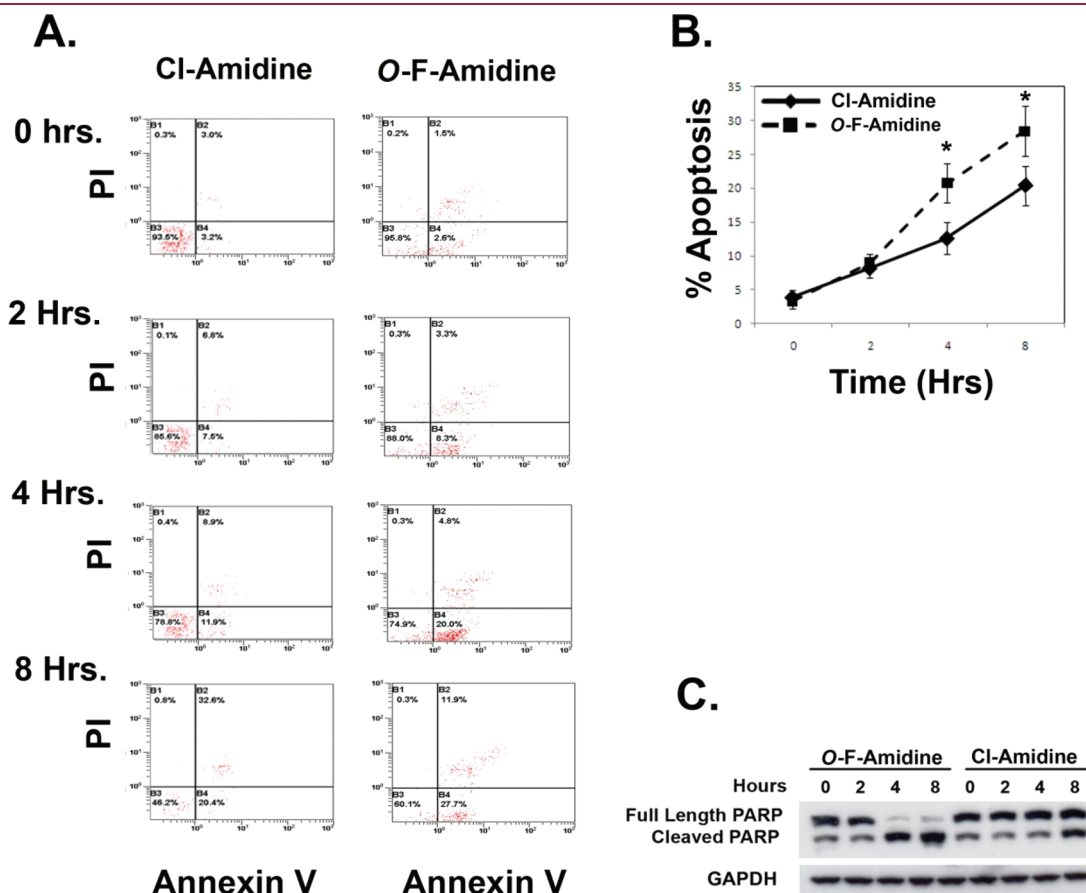


Figure 8. *o*-F-amidine is more potent at driving apoptosis in inflammatory cells than Cl-amidine. TK6 cells, a human lymphoblastoid cell line, were exposed to either Cl-amidine (50 μ g/mL) or *o*-F-amidine (50 μ g/mL) for indicated time periods. (A) Representative scatterplots from one of three separate experiments. (B) Average percentage apoptosis (from percentages in the 4th quadrant) for Cl-amidine and *o*-F-amidine as indicated from 3 experiments. (C) PARP cleavage by Cl-amidine and *o*-F-amidine.

11-, 20-, 39-, and 65-fold for PADs 4, 2, 3, and 1, respectively. The observed warhead dependence on k_{inact}/K_i likely reflects differences in the ability to position the warhead for nucleophilic attack by the active site cysteine. This result is significant because it suggests that the warhead itself can act as a selectivity determinant. Consistent with this notion are the interisozyme selectivity data. For example, relative to Cl-amidine, the inclusion of the *ortho*-carboxylate in *o*-Cl-amidine actually decreases the selectivity for PADs 2 and 3 by 2- to 3-fold. In contrast, with *o*-F-amidine the selectivity trends are the reverse, as the k_{inact}/K_i values are increased by 2- to 3-fold for PADs 2 and 3 (to 24- and 27-fold, respectively) and 6-fold for PAD4. Given these results, *o*-Cl-amidine is a PAD1 and 4 selective inhibitor, whereas *o*-F-amidine is primarily a PAD1 selective inhibitor. This preference for PAD1 suggests that *o*-F-amidine will serve as a versatile tool that can be used to assign physiological functions to PAD1. On the basis of the crystallographic data, as well as mutagenesis studies, the enhanced potency and selectivity is likely due to interactions between the *ortho*-carboxylate and the indole nitrogen of W347 of PAD4. In cellulo studies indicate that these two compounds are better than F- and Cl-amidine in their ability to inhibit histone deimination, trigger HL-60 cell differentiation, and potentiate the cell killing effects of doxorubicin in HL-60 cells in a synergist and dose dependent fashion. Finally, *o*-F-amidine induces apoptosis of inflammatory cells to a greater extent than Cl-amidine. Given these findings, the incorporation of a carboxylate at this position will likely prove to be an important feature of third and fourth generation PAD inhibitors. Future studies will focus on evaluating the efficacy of *o*-F- and *o*-Cl-amidine in mouse models of RA, colitis, and cancer.

EXPERIMENTAL SECTION

Chemicals. Cl-amidine (1), F-amidine (2), and 2-fluoroacetamidine (3) were synthesized as previously described.^{41,42} PADs 1–4 were purified as previously described.^{4,43} Cell culture media, RPMI 1640, and fetal bovine serum were obtained from ThermoScientific (Pittsburgh, PA). All compounds were purified to $\geq 95\%$ purity. Purity was assessed by HPLC.

2-Fluoro-*N*-propylacetamidine · HCl (4). To a solution of ethyl 2-fluorothioacetimidate (174 mg, 1.0 mmol) in dry ethanol (3 mL) at 0 °C was added propylamine (59 mg, 1.0 mmol). After 10 min, the reaction was allowed to warm to rt, and stirring was continued for an additional 50 min. The mixture was partitioned between ether (3 mL) and H₂O (5 mL); the aqueous layer was separated and lyophilized to yield the title compound as an off-white solid (134 mg, 87%). ¹H NMR (400 MHz, D₂O) δ (ppm): 5.07 (d, $J_{\text{HF}} = 45.2$ Hz, 2H), 3.10 (t, $J = 7.2$ Hz, 2H), 1.46 (q, $J = 7.2$ Hz, 2H), 0.73 (t, $J = 7.2$ Hz, 3H). ¹³C NMR (100 MHz, D₂O) δ (ppm): 162.21 (d, $J_{\text{CF}} = 19.8$ Hz), 77.53 (d, $J_{\text{CF}} = 177.4$ Hz), 43.65, 20.15, 10.30. HRMS (ESI) m/z calculated for [C₅H₁₂FN₂⁺], 119.0984; observed, 119.0993.

***N*-Benzyl-2-fluoroacetimidamide · HCl (5).** To a solution of ethyl 2-fluorothioacetimidate (174 mg, 1.0 mmol) in dry ethanol (3 mL) at 0 °C was added benzylamine (107 mg, 1.0 mmol). After 10 min, the reaction was allowed to warm to rt, and stirring was continued for an additional 50 min. The mixture was partitioned between ether (3 mL) and H₂O (5 mL); the aqueous layer was separated and lyophilized to yield the title compound as a white powder (147 mg, 73%). ¹H NMR (300 MHz, D₂O) δ (ppm): 7.29 (m, 5H), 5.18 (d, $J_{\text{HF}} = 45$ Hz, 2H), 4.44 (s, 2H). ¹³C NMR (75 MHz, D₂O) δ (ppm): 162.82 (d, $J_{\text{CF}} = 19.8$ Hz), 133.84, 129.27, 128.67, 127.84, 77.85 (d, $J_{\text{CF}} = 177.45$ Hz), 45.74. HRMS (ESI) m/z calculated for [C₉H₁₂FN₂⁺], 167.0984; observed, 167.0979.

2-Fluoro-*N*-phenylacetimidamide · HCl (6). To a solution of ethyl 2-fluorothioacetimidate (174 mg, 1.0 mmol) in dry ethanol (3 mL) at 0 °C was added aniline (93 mg, 1.0 mmol). After 10 min, the reaction was allowed to warm to rt, and stirring was continued for an additional 50 min. The mixture was partitioned between ether (3 mL) and H₂O (5 mL); the aqueous layer was separated and lyophilized to yield the title compound as an off-white solid (150 mg, 80%). ¹H NMR (300 MHz, D₂O) δ (ppm): 7.50–7.35 (m, 3H), 7.25 (m, 2H), 5.36 (d, $J_{\text{HF}} = 44.7$ Hz, 2H). ¹³C NMR (75 MHz, D₂O) δ (ppm): 163.52 (d, $J_{\text{CF}} = 19.8$ Hz), 133.28, 130.94, 127.56, 125.31, 77.86 (d, $J_{\text{CF}} = 179.1$ Hz). HRMS (ESI) m/z calculated for [C₈H₁₀FN₂⁺], 153.0820; observed, 153.0832.

***N*¹-Benzoyl-(3-(2-fluoroacetimidamido))-L-phenylalanine Amide · TFA (7).** Rink AM Amide resin (300 mg, 0.2 mmol) was treated twice with 5 mL of 20% piperidine (in DMF) for 20 min and subsequently washed with dry DMF (3 \times 5 mL). Fmoc-(3-nitro)Phe-OH (100 mg, 0.23 mmol), HOTT (S-(1-oxido-2-pyridyl)-thio-*N,N,N'*, *N'*-tetramethyluronium hexafluorophosphate; 303 mg, 0.35 mmol), and triethylamine (0.064 mL, 0.46 mmol) were dissolved in dry DMF (3 mL) and allowed to react for 10 min before being added to the resin. The reaction mixture was rocked at rt for 3 h before the resin was filtered and washed with DMF (3 \times 5 mL). The resin was treated with acetic anhydride (0.19 mL, 2.0 mmol) and triethylamine (0.56 mL, 4.0 mmol) in DMF (5 mL) for 2 h to cap any remaining amino groups on the resin. The resin was collected by filtration, washed with DMF (2 \times 5 mL), and treated twice for 20 min with 5 mL of 20% piperidine in DMF. The resin was then washed with DMF (3 \times 5 mL), resuspended in DMF (5 mL), and treated with benzoyl chloride (0.093 mL, 0.8 mmol) and triethylamine (0.22 mL, 1.6 mmol) and rocked at rt overnight. The resin was washed with DMF (3 \times 5 mL), then treated overnight at rt with 2 M tin(II)chloride (6 mL), collected by filtration, and washed with DMF (3 \times 5 mL). The resin was then treated overnight with a solution of ethyl 2-fluorothioacetimidate (128 mg, 0.8 mmol) in DMF (5 mL), then collected by filtration, washed with DMF (3 \times 5 mL), ethanol (3 \times 5 mL), and DCM (3 \times 5 mL), and dried for 1 h under reduced pressure. The dry resin was treated three times (1 h each) with 5 mL of TFA/TIS/H₂O (95/2.5/2.5). The filtrates were collected, combined, and concentrated. Cold ether (25 mL) was added to the remaining residue, and the resulting precipitate was collected by centrifugation and purified by RP-HPLC to yield the title compound as an off-white solid (16.5 mg, 18%). ¹H NMR (400 MHz, D₂O) δ (ppm): 7.52 (m, 3H), 7.36 (m, 4H), 7.14 (m, 2H), 5.28 (d, $J_{\text{HF}} = 44.4$ Hz), 4.72 (dd, $J = 5.6, 9.6$ Hz, 1H), 3.26 (dd, $J = 5.6, 14.0$ Hz, 1H), 2.97 (dd, $J = 10.0, 14.0$ Hz, 1H). ¹³C NMR (100 MHz, D₂O) δ (ppm): 175.80, 170.63, 163.26 (d, $J_{\text{CF}} = 19.1$ Hz), 139.42, 132.61, 132.45, 132.29, 130.50, 130.38, 128.65, 127.03, 126.04, 123.99, 77.60 (d, $J_{\text{CF}} = 178.8$ Hz), 54.71, 36.65. HRMS (ESI) m/z calculated for [C₁₈H₂₀FN₄O₂⁺], 343.1570; observed, 343.1565.

***N*¹-Benzoyl-(3-(2-fluoroacetimidamido))-L-phenylglycine Amide · TFA (8).** Rink AM Amide resin (300 mg, 0.2 mmol) was treated twice with 5 mL of 20% piperidine (in DMF) for 20 min and subsequently washed with dry DMF (3 \times 5 mL). Bz-(3-NO₂)Phg-OH (180 mg, 0.6 mmol), HBTU (2-(1*H*-benzotriazol-1-yl)-1,1,3,3-tetramethyluronium hexafluorophosphate; 228 mg, 0.6 mmol), HOBt (92 mg, 0.6 mmol), and triethylamine (0.17 mL, 1.2 mmol) were dissolved in dry DMF (5 mL) and allowed to react for 10 min before being added to the resin. The reaction mixture was rocked at rt for 3 h before the resin was collected by filtration and washed with DMF (3 \times 5 mL). The resin was rocked overnight at rt in 2 M tin(II)chloride (6 mL), collected by filtration, and washed with DMF (3 \times 5 mL). The resin was then treated overnight with a solution of ethyl 2-fluorothioacetimidate (128 mg, 0.8 mmol) in DMF (5 mL), then collected by filtration, washed with DMF (3 \times 5 mL), ethanol (3 \times 5 mL), and DCM (3 \times 5 mL), and dried for 1 h under reduced pressure. The dry resin was treated three times (1 h each)

with 5 mL of TFA/TIS/H₂O (95/2.5/2.5). The filtrates were collected, combined, and concentrated. Cold ether (25 mL) was added to the remaining residue, and the resulting precipitate was collected by centrifugation and purified by RP-HPLC to yield the title compound as a white powder (19.5 mg, 22%). ¹H NMR (400 MHz, D₂O) δ (ppm): 7.64 (m, 2H), 7.48 (m, 3H), 7.36 (m, 3H), 7.28 (m, 1H), 5.54 (s, 1H), 5.34 (d, *J*_{HF} = 44.8 Hz, 2H). ¹³C NMR (100 MHz, D₂O) δ (ppm): 175.11, 173.95, 170.42, 163.54 (d, *J*_{CF} = 19.8 Hz), 138.40, 132.98, 132.60, 132.55, 131.21, 129.70, 128.76, 127.36, 125.97, 124.87, 120.11, 77.69 (d, *J*_{CF} = 178.1 Hz), 57.63. HRMS (ESI) *m/z* calculated for [C₁₇H₁₈FN₄O₂⁺], 329.1414; observed, 329.1417.

N¹-Benzoyl-(4-(2-fluoroacetimidamido))-L-phenylalanine Amide·TFA (9). Rink AM Amide resin (300 mg, 0.2 mmol) was treated twice with 5 mL of 20% piperidine (in DMF) for 20 min and subsequently washed with dry DMF (3 × 5 mL). Fmoc-(4-nitro)Phe-OH (100 mg, 0.23 mmol), HOTT (303 mg, 0.35 mmol), and triethylamine (0.064 mL, 0.46 mmol) were dissolved in dry DMF (3 mL) and allowed to react for 10 min before being added to the resin. The reaction mixture was rocked at rt for 3 h before the resin was filtered and washed with DMF (3 × 5 mL). The resin was treated with acetic anhydride (0.19 mL, 2.0 mmol) and triethylamine (0.56 mL, 4.0 mmol) in DMF (5 mL) for 2 h to cap any remaining amino groups on the resin. The resin was collected by filtration, washed with DMF (2 × 5 mL), and treated twice for 20 min with 5 mL of 20% piperidine (in DMF). The resin was then washed with DMF (3 × 5 mL), resuspended in DMF (5 mL), and treated with benzoyl chloride (0.093 mL, 0.8 mmol) and triethylamine (0.22 mL, 1.6 mmol), and rocked at rt overnight. The resin was washed with DMF (3 × 5 mL) then treated overnight at rt with 2 M tin(II)chloride (6 mL), collected by filtration, and washed with DMF (3 × 5 mL). The resin was then treated overnight with a solution of ethyl 2-fluorothioacetimidate (128 mg, 0.8 mmol) in DMF (5 mL), then collected by filtration, washed with DMF (3 × 5 mL), ethanol (3 × 5 mL), and DCM (3 × 5 mL), and dried for 1 h under reduced pressure. The dry resin was treated three times (1 h each) with 5 mL of TFA/TIS/H₂O (95/2.5/2.5). The filtrates were collected, combined, and concentrated. Cold ether (25 mL) was added to the remaining residue, and the resulting precipitate was collected by centrifugation and purified by RP-HPLC to yield the title compound as an off-white solid. ¹H NMR (400 MHz, CD₃OD) δ (ppm): 7.76 (d, *J* = 8.3 Hz, 2H), 7.55–7.49 (m, 3H), 7.44 (m, 2H), 7.29 (d, *J* = 8.3 Hz, 2H), 5.43 (d, *J*_{HF} = 45.2 Hz), 3.66–3.48 (m, 1H), 3.36 (dd, *J* = 4.8, 13.8 Hz, 1H), 3.09 (dd, *J* = 9.4, 13.5 Hz, 1H). ¹³C NMR (100 MHz, D₂O) δ (ppm): 175.99, 170.18, 164.99 (d, *J*_{CF} = 19.4 Hz), 140.78, 135.25, 133.15, 132.56, 129.74, 128.55, 126.66, 80.20, 78.42 (d, *J*_{CF} = 179.9 Hz), 56.16, 38.93. HRMS (ESI) *m/z* calculated for [C₁₈H₂₀FN₄O₂⁺], 343.1570; observed, 343.1570.

N¹-Benzoyl-4-((2-fluoro-1-iminoethyl)aminomethyl)-L-phenylalanine Amide·TFA (10). Rink AM Amide resin (300 mg, 0.186 mmol) was preswelled in DMF (5 mL) for 1 h, filtered, washed with DMF (2 × 5 mL), treated with 20% piperidine (in DMF) (2 × 5 mL) for 20 min, and subsequently washed with dry DMF (3 × 5 mL). Fmoc-L-(4-amino(Boc)methyl)Phe-OH (384 mg, 0.744 mmol), HBTU (282 mg, 0.744 mmol), and HOBt (114 mg, 0.744 mmol) were dissolved in DMF (3 mL) and allowed to stand at rt for 10 min before *N*-methylmorpholine (0.4 M in DMF) (3.7 mL, 1.49 mmol) was added. The reaction mixture was rocked at rt for 3 h before the resin was filtered, washed with DMF (3 × 5 mL), and treated with 20% piperidine (in DMF) (2 × 5 mL) for 1 h and subsequently filtered and washed with DMF (3 × 5 mL). A mixture of benzoyl chloride (105 mg, 0.744 mmol) and *N*-methylmorpholine (0.4 M in DMF) (3.7 mL, 1.49 mmol) was added to the resin, and this suspension was rocked at rt. After 16 h, the resin was collected by filtration and washed with DMF (3 × 5 mL), ethanol (2 × 5 mL), and DCM (2 × 5 mL) and dried overnight under reduced pressure. The dry resin was treated twice with a mixture of

TFA/TIS/H₂O (95/2.5/2.5) at rt for 3 h. The resulting filtrates were collected, combined, and concentrated under a stream of nitrogen. Cold ether (20 mL) was added to the remaining residue, and the resulting precipitate was collected by centrifugation and purified by RP-HPLC to afford *N*-α-benzoyl-L-(4-aminomethyl)phenylalanine amide. Ethyl fluoroacetimidate hydrochloride (10 mg, 0.073 mmol), dry triethylamine (0.004 mL, 0.029 mmol), and *N*-α-benzoyl-L-(4-aminomethyl)phenylalanine amide (6 mg, 0.015 mmol) were dissolved in dry DMF (1 mL), and the mixture was stirred under nitrogen for 16 h. Purification by RP-HPLC afforded the title compound as a hygroscopic white powder upon lyophilization. ¹H NMR (400 MHz, CD₃OD) δ (ppm): 7.63 (d, *J* = 7.7 Hz, 2H), 7.42 (t, *J* = 7.4 Hz, 1H), 7.33 (t, *J* = 7.6 Hz, 2H), 7.28 (d, *J* = 8.0 Hz, 2H), 7.19 (d, *J* = 8.0 Hz, 2H), 5.13 (d, *J* = 45.4 Hz, 2H), 4.73 (dd, *J* = 5.5, 10.0 Hz, 1H, obtained in D₂O, 500 MHz), 4.40 (s, 2H), 3.27 (dd, *J* = 5.4, 13.9 Hz, 1H, obtained in D₂O, 400 MHz), 2.94 (dd, *J* = 9.9, 13.9 Hz, 1H). ¹³C NMR (100 MHz, CD₃OD) δ (ppm): 175.87, 170.78, 162.63 (d, *J*_{CF} = 18.9 Hz), 137.13, 132.85, 132.42, 132.38, 129.78, 128.68, 127.80, 127.11, 77.62 (d, *J*_{CF} = 177.3 Hz), 55.03, 45.16, 36.79. HRMS (ESI) *m/z* calculated for [C₁₉H₂₂FN₄O₂⁺], 357.1227; observed, 357.1732.

N¹-Benzoyl-N⁴-(2-fluoro-1-iminoethyl)-1,4-diaminobutane·TFA (11). To a solution of N¹-benzoyl-1,4-diaminobutane·TFA (39 mg, 0.13 mmol) in dry methanol (3 mL) was added ethyl 2-fluorothioacetimidate (36 mg, 0.25 mmol) and Cs₂CO₃ (62 mg, 0.19 mmol). The reaction was allowed to stir at rt overnight before being quenched with TFA. The mixture was subsequently diluted with H₂O and purified by RP-HPLC to yield the title compound as a clear colorless residue (46.5 mg, 100%). ¹H NMR (300 MHz, D₂O) δ (ppm): 7.60–7.30 (m, 5H), 5.07 (d, *J*_{HF} = 44.7 Hz, 2H), 3.26 (m, 4H), 1.47 (m, 4H). ¹³C NMR (100 MHz, D₂O) δ (ppm): 170.83, 162.34 (*J*_{CF} = 19.8 Hz), 133.51, 131.97, 128.65, 126.82, 77.49 (*J*_{CF} = 177.4 Hz), 41.61, 39.06, 25.67, 23.95. HRMS (ESI) *m/z* calculated for [C₁₃H₁₉FN₃O⁺], 252.1512; observed, 252.1517.

N¹-Benzenesulfonyl-N⁴-(2-fluoro-1-iminoethyl)-1,4-diaminobutane·TFA (12). To a solution of N¹-benzenesulfonyl-1,4-diaminobutane·TFA (43 mg, 0.13 mmol) in dry methanol (3 mL) was added ethyl 2-fluorothioacetimidate (36 mg, 0.25 mmol) and Cs₂CO₃ (62 mg, 0.19 mmol). The reaction was allowed to stir at rt overnight before being quenched with TFA. The mixture was subsequently diluted with H₂O and purified by RP-HPLC to yield the title compound as a clear colorless residue (41.5 mg, 80%). ¹H NMR (300 MHz, D₂O) δ (ppm): 7.72 (m, 2H), 7.51 (m, 3H), 5.07 (d, *J*_{HF} = 44.7 Hz, 2H), 3.08 (t, *J* = 6.9 Hz, 2H), 2.75 (t, *J* = 6.8 Hz, 2H), 1.45 (m, 4H). ¹³C NMR (75 MHz, D₂O) δ (ppm): 162.50 (d, *J*_{CF} = 19.3 Hz), 138.36, 133.65, 129.68, 126.76, 77.69 (d, *J*_{CF} = 177.45 Hz), 42.23, 41.66, 25.99, 23.94. HRMS (ESI) *m/z* calculated for [C₁₂H₁₉FN₃O₂S⁺], 288.1182; observed, 288.1183.

N¹-Benzenesulfonyl-N⁵-(2-fluoro-1-iminoethyl)-L-ornithine Amide·TFA (13). Rink AM Amide resin (500 mg, 0.36 mmol) was preswelled in DMF (15 mL) for 1 h, filtered, washed with DMF (2 × 15 mL), treated with 20% piperidine (in DMF) (2 × 15 mL) for 20 min, and subsequently washed with dry DMF (3 × 15 mL). Fmoc-Orn-(Dde)-OH (552 mg, 1.07 mmol), HBTU (404 mg, 1.07 mmol), and HOBt (163 mg, 1.07 mmol) were dissolved in DMF (5 mL) and allowed to stand at rt for 10 min before *N*-methylmorpholine (0.4 M in DMF) (5.3 mL, 2.13 mmol) was added. The reaction mixture was rocked at rt for 16 h before the resin was filtered, washed with DMF (3 × 5 mL), and treated with 20% piperidine (in DMF) (2 × 15 mL) for 1 h and subsequently filtered and washed with DMF (3 × 15 mL). A mixture of benzenesulfonyl chloride (215 mg, 1.42 mmol) and *N*-methylmorpholine (0.4 M in DMF) (7 mL, 2.84 mmol) was added to the resin, and this suspension was rocked at rt. After 16 h, the resin was collected by filtration and washed with DMF (3 × 15 mL). The resin was treated with 2% hydrazine (in DMF) (15 mL) for 2 h, washed with DMF

(3 × 15 mL), ethanol (2 × 15 mL), and DCM (2 × 15 mL), collected by filtration, and dried overnight under reduced pressure. Ethyl fluoroacetimidate hydrochloride (390 mg, 2.77 mmol) and dry triethylamine (0.38 mL, 2.77 mmol) were added to the resin suspended in DMF (15 mL), and the mixture was stirred under nitrogen for 16 h. The resin was collected by filtration and washed sequentially with DMF (3 × 15 mL), ethanol (2 × 15 mL), and DCM (2 × 15 mL). The resin was incubated three times with a mixture of TFA (10%) and TIS (1%) in DCM for 1 h each. The filtrates were collected, combined, and concentrated under a stream of nitrogen. Cold ether (20 mL) was added to the remaining residue, and the resulting precipitate was collected by centrifugation. This precipitate was washed with cold ether (2 × 15 mL) and lyophilized. Purification by RP-HPLC afforded the title compound as a hygroscopic white powder upon lyophilization. ¹H NMR (400 MHz, CD₃OD) δ (ppm): 7.89 (d, *J* = 8.4 Hz, 2H), 7.65–7.55 (m, 3H), 5.27 (d, *J* = 45.4 Hz, 2H), 3.82 (m, 1H), 3.10 (m, 2H, obtained in D₂O, 400 MHz), 1.81–1.59 (m, 4H). ¹³C NMR (100 MHz, CD₃OD) δ (ppm): 175.68, 164.28 (d, *J*_{CF} = 19.5 Hz), 141.86, 133.93, 130.24, 128.17, 78.96 (d, *J*_{CF} = 177.9 Hz), 57.13, 42.78, 31.56, 24.73. HRMS (ESI) *m/z* calculated for [C₁₃H₂₀FN₄O₃S⁺], 331.1240; observed, 331.1237.

N¹-(4-Carbonyl)imidazole-N⁵-(2-fluoro-1-iminoethyl)-L-ornithine Amide · TFA (14). Rink AM Amide resin (300 mg, 0.2 mmol) was treated twice with 5 mL of 20% piperidine (in DMF) for 20 min and subsequently washed with dry DMF (3 × 5 mL). Fmoc-Orn(Dde)-OH (414 mg, 0.8 mmol), HBTU (303 mg, 0.8 mmol), HOBt (122 mg, 0.8 mmol), and triethylamine (0.22 mL, 1.6 mmol) were dissolved in dry DMF (5 mL) and allowed to react for 10 min before being added to the resin. The reaction mixture was rocked at rt for 3 h before the resin was filtered, washed with DMF (3 × 5 mL), treated twice with 5 mL of 20% piperidine (in DMF) for 20 min, and washed with dry DMF (3 × 5 mL). 1*H*-imidazole-4-carbonyl chloride · HCl (134 mg, 0.8 mmol) and triethylamine (0.22 mL, 1.6 mmol) were dissolved in dry DMF (5 mL) and added to the resin. After rocking overnight at rt, the resin was collected by filtration, washed with DMF (3 × 5 mL), and treated twice with 2% hydrazine (in DMF) (5 mL) for 1 h to remove the Dde-protecting group. A solution of ethyl 2-fluoroacetimidate · HCl (113 mg, 0.8 mmol) and triethylamine (0.22 mL, 1.6 mmol) in DMF (5 mL) was added to the resin, and the mixture was rocked at rt. After 16 h, the resin was collected by filtration, washed with DMF (3 × 5 mL), ethanol (3 × 5 mL), and DCM (3 × 5 mL), then dried under reduced pressure for 1 h. The dry resin was treated three times (1 h each) with 5 mL of TFA/TIS/H₂O (95/2.5/2.5). The filtrates were collected, combined, and concentrated. Cold ether (25 mL) was added to the remaining residue, and the resulting precipitate was collected by centrifugation and purified by RP-HPLC to yield the title compound as a white powder (49 mg, 48%). ¹H NMR (400 MHz, D₂O) δ (ppm): 8.65 (s, 1H), 7.92 (s, 1H), 5.10 (d, *J*_{HF} = 44.8 Hz, 2H), 4.33 (dd, *J* = 5.6, 8.4 Hz, 1H), 3.24 (t, *J* = 6.8 Hz, 2H), 1.89–1.58 (m, 4H). ¹³C NMR (100 MHz, D₂O) δ (ppm): 175.77, 162.54 (d, *J*_{CF} = 19.1 Hz), 158.74, 135.42, 126.44, 123.44, 120.75, 117.64, 114.74, 77.51 (d, *J*_{CF} = 177.4 Hz), 53.38, 41.32, 27.95, 23.17. HRMS (ESI) *m/z* calculated for [C₁₁H₁₈FN₆O₂⁺], 285.1475; observed, 285.1468.

N¹-(3-Carbonyl)pyrrole-N⁵-(2-fluoro-1-iminoethyl)-L-ornithine Amide · TFA (15). N¹-(3-Carbonyl)pyrrole-L-ornithine amide · TFA (18 mg, 0.053 mmol), ethyl 2-fluoroacetimidate (15 mg, 0.11 mmol), and Cs₂CO₃ (26 mg, 0.080 mmol) were dissolved in dry methanol (1 mL). The reaction was stirred at rt for 16 h, quenched with TFA, diluted with H₂O, and purified by RP-HPLC to yield the title compound as a white solid (11 mg, 54%). ¹H NMR (400 MHz, D₂O) δ (ppm): 10.78 (br, 1H), 6.95 (s, 1H), 6.78 (s, 1H), 6.19 (s, 1H), 5.10 (d, *J*_{HF} = 44.8 Hz, 2H), 4.30 (dd, *J* = 4.8, 8.4 Hz, 1H), 3.25 (t, *J* = 6.8 Hz, 2H), 1.95–1.59 (m, 4H). ¹³C NMR (100 MHz, D₂O) δ (ppm): 176.89, 175.71, 162.53 (d, *J*_{CF} = 19.1 Hz), 123.97, 123.69, 112.13, 109.63, 77.52 (d, *J*_{CF} = 178.1 Hz), 52.91, 41.32, 28.05, 23.26. HRMS (ESI) *m/z* calculated for [C₁₂H₁₉FN₅O₂⁺], 284.1523; observed, 284.1526.

N¹-(2-Hydroxy-5-nitro)benzoyl-N⁵-(2-fluoro-1-iminoethyl)-L-ornithine Amide · TFA (16). To a solution of N¹-(2-hydroxy-5-nitro)benzoyl-L-ornithine · TFA (13.7 mg, 0.033 mmol) in dry methanol (1 mL) was added ethyl 2-fluoroacetimidate (9.4 mg, 0.067 mmol) and Cs₂CO₃ (16.3 mg, 0.049 mmol). The reaction was stirred overnight at rt, quenched with TFA, diluted with H₂O, and purified by RP-HPLC to yield the title compound as a white powder (14.7 mg, 95%). ¹H NMR (400 MHz, D₂O) δ (ppm): 8.45 (d, *J* = 3.2 Hz, 1H), 8.05 (dd, *J* = 2.8, 9.2 Hz, 1H), 6.88 (d, *J* = 9.2 Hz, 1H), 5.11 (d, *J*_{HF} = 44.8 Hz, 2H), 4.39 (dd, *J* = 5.6, 8.4 Hz, 1H), 3.27 (t, *J* = 6.8 Hz, 2H), 1.95–1.61 (m, 4H). ¹³C NMR (100 MHz, D₂O) δ (ppm): 175.95, 166.95, 162.55 (d, *J*_{CF} = 20.5 Hz), 139.85, 128.96, 125.98, 117.69, 117.13, 77.53 (d, *J*_{CF} = 177.4 Hz), 53.32, 41.32, 28.31, 23.05. HRMS (ESI) *m/z* calculated for [C₁₄H₁₈FN₅O₅⁺], 356.1370; observed, 356.1359.

N-α-(2-Carboxyl)benzoyl-N⁵-(2-fluoro-1-iminoethyl)-L-ornithine Amide (o-F-amidine) (17). Rink Amide AM resin (300 mg, 0.186 mmol) was suspended in 20% piperidine (in DMF) (5 mL) and gently rocked at rt for 20 min. The suspension was filtered and treated with 20% piperidine once more. After 20 min, the resin was filtered and washed with DMF (3 × 5 mL). Fmoc-Orn(Boc)-OH (338 mg, 0.74 mmol), HBTU (282 mg, 0.74 mmol), and HOBt (114 mg, 0.74 mmol) were dissolved in DMF (5 mL), and *N*-methylmorpholine (0.164 mL, 1.49 mmol) was added. After 10 min, this solution was added to the resin followed by gentle rocking. After 3 h, the resin was filtered, washed with DMF (3 × 5 mL), and treated with 20% piperidine (2 × 5 mL). The resin was then filtered, washed with DMF (3 × 5 mL), and resuspended in DMF (5 mL). After the addition of phthalic anhydride (110 mg, 0.74 mmol) and triethylamine (0.207 mL, 1.49 mmol), the mixture was rocked at rt for 16 h. The resin was collected by filtration, washed with DMF (3 × 5 mL), ethanol (2 × 5 mL), and dichloromethane (2 × 5 mL), dried under reduced pressure, and treated twice with a mixture of TFA/TIS/H₂O (95/2.5/2.5) for 1 h. The filtrates were collected, combined, and concentrated under a stream of nitrogen. Cold ether (20 mL) was added to the remaining residue, and the resulting precipitate was collected by centrifugation, washed twice with ether (10 mL), and lyophilized. This precipitate (15 mg, 0.038 mmol), ethyl chloroacetimidate hydrochloride (10.7 mg, 0.076 mmol), and cesium carbonate (18.5 mg, 0.057 mmol) were dissolved in dry methanol (1 mL) and stirred at rt for 16 h. The reaction was quenched with TFA, diluted with H₂O, and purified by RP-HPLC to afford the title compound as a hygroscopic white powder (15 mg, 23%). ¹H NMR (400 MHz, D₂O) δ (ppm): 7.83 (m, 1H), 7.56–7.45 (m, 2H), 7.35 (m, 1H), 4.34 (m, 1H), 3.25 (m, 2H), 1.92–1.55 (m, 4H). ¹³C NMR (100 MHz, D₂O) δ (ppm): 176.04, 173.00, 170.28, 162.79, 135.99, 135.10, 132.56, 131.51, 130.41, 128.62, 127.39, 53.32, 41.87, 39.05, 27.89, 23.04. HRMS (ESI) *m/z* calculated for [C₁₅H₂₀ClN₄O₄⁺], 355.1173; observed, 355.1172.

N-α-(2-Carboxyl)benzoyl-N⁵-(2-chloro-1-iminoethyl)-L-ornithine Amide (o-Cl-amidine) (18). Rink Amide AM resin (300 mg, 0.186 mmol) was suspended in 20% piperidine (in DMF) (5 mL) and gently rocked at rt for 20 min. The suspension was filtered and treated with 20% piperidine once more. After 20 min, the resin was filtered and washed with DMF (3 × 5 mL). Fmoc-Orn(Boc)-OH (338 mg, 0.74 mmol), HBTU (282 mg, 0.74 mmol), and HOBt (114 mg, 0.74 mmol) were dissolved in DMF (5 mL), and *N*-methylmorpholine (0.164 mL, 1.49 mmol) was added. After 10 min, this solution was added to the resin followed by gentle rocking. After 3 h, the resin was filtered, washed with DMF (3 × 5 mL), and treated with 20% piperidine (2 × 5 mL). The resin was then filtered, washed with DMF (3 × 5 mL), and resuspended in DMF (5 mL). After the addition of phthalic anhydride (110 mg, 0.74 mmol) and triethylamine (0.207 mL, 1.49 mmol), the mixture was rocked at rt for 16 h. The resin was collected by filtration, washed with DMF (3 × 5 mL), ethanol (2 × 5 mL), and dichloromethane (2 × 5 mL), dried under reduced pressure, and treated twice with a mixture of TFA/TIS/H₂O (95/2.5/2.5) for 1 h. The filtrates were collected,

combined, and concentrated under a stream of nitrogen. Cold ether (20 mL) was added to the remaining residue, and the resulting precipitate was collected by centrifugation, washed twice with ether (10 mL), and lyophilized. This precipitate (11.0 mg, 0.028 mmol), ethyl fluoroacetimidate hydrochloride (8.8 mg, 0.056 mmol), and cesium carbonate (13.7 mg, 0.042 mmol) were dissolved in dry methanol (1 mL) and stirred at rt for 16 h. The reaction was quenched with TFA, diluted 2-fold with H₂O, and purified by RP-HPLC to afford the title compound as a hygroscopic white powder (18 mg, 29%). ¹H NMR (400 MHz, D₂O) δ (ppm): 7.84 (m, 1H), 7.56–7.44 (m, 2H), 7.39 (m, 1H), 5.12 (d, *J*_{HF} = 44.8 Hz, 2H), 4.34 (m, 1H), 3.25 (m, 2H), 1.92–1.59 (m, 4H). ¹³C NMR (100 MHz, D₂O) δ (ppm): 176.01, 172.92, 169.70, 162.56 (d, *J*_{CF} = 19.8 Hz), 136.19, 132.85, 131.72, 130.39, 128.65, 127.42, 77.53 (d, *J*_{CF} = 177.4 Hz), 53.35, 41.32, 27.90, 23.18. HRMS (ESI) *m/z* calculated for [C₁₅H₂₀FN₄O₄⁺], 339.1468; observed, 339.1468.

Ethyl 2-Fluorothioacetimidate (19). 2-Fluoroacetonitrile (561 mg, 9.5 mmol) and ethanethiol (1180 mg, 19 mmol) were added to 15 mL of 1 M HCl (in ether) at 0 °C. The reaction was stirred overnight at 4 °C. The product, which precipitated from the solution, was collected by centrifugation, washed with cold ether (3 × 10 mL), and dried under vacuum for 3 h to yield the title compound as a white crystalline compound (926 mg, 56%).

N¹-Benzoyl-3-(2-fluoroacetimidamido)-L-phenylalanine Amide·TFA (20). Rink AM Amide resin (300 mg, 0.213 mmol) was pressed in DMF (5 mL) for 1 h, filtered, washed with DMF (2 × 5 mL), treated with 20% piperidine (in DMF) (2 × 5 mL) for 20 min, and subsequently washed with dry DMF (3 × 5 mL). Fmoc-Phe(3-NO₂)-OH (368 mg, 0.852 mmol), HBTU (323 mg, 0.852 mmol), and HOBt (130 mg, 0.852 mmol) were dissolved in DMF (2.3 mL) and allowed to stand at rt for 10 min before *N*-methylmorpholine (0.4 M in DMF) (4.2 mL, 1.70 mmol) was added. The reaction mixture was rocked at rt for 3 h before the resin was filtered, washed with DMF (3 × 5 mL), and treated with 20% piperidine (in DMF) (2 × 5 mL) for 1 h and subsequently filtered and washed with DMF (3 × 5 mL). A mixture of benzoyl chloride (0.1 mL, 0.852 mmol) and *N*-methylmorpholine (0.4 M in DMF) (4.3 mL, 1.70 mmol) was added to the resin, and this suspension was rocked at rt. After 16 h, the resin was collected by filtration and washed with DMF (3 × 5 mL), rocked in a solution of tin(II)chloride (6 mL, 2 M in DMF) for 24 h, collected by filtration, washed with DMF (3 × 5 mL), ethanol (2 × 5 mL), and DCM (2 × 5 mL), and dried overnight under reduced pressure. The resin was resuspended in dry DMF (5 mL) and treated with ethyl fluoroacetimidate hydrochloride (282 mg, 2 mmol) and dry triethylamine (0.28 mL, 2 mmol) under nitrogen for 16 h, and subsequently collected by filtration and washed with DMF (3 × 5 mL), ethanol (2 × 5 mL), and DCM (2 × 5 mL), and dried under reduced pressure. Cleavage from the resin was accomplished by treatment with a mixture of TFA (10%) and TIS (1%) in DCM (10 mL) for 10 min. This treatment was repeated, and both filtrates were collected, combined, and concentrated under a stream of nitrogen. Cold ether (20 mL) was added to the remaining residue, and the resulting precipitate was collected by centrifugation, washed twice with ether (10 mL), lyophilized, and purified by RP-HPLC to afford the title compound as a hygroscopic white powder upon lyophilization. ¹H NMR (400 MHz, CD₃OD) δ (ppm): 7.76 (d, *J* = 8.3 Hz, 2H), 7.55–7.49 (m, 3H), 7.44 (m, 2H), 7.29 (d, *J* = 8.3 Hz, 2H), 5.43 (d, *J* = 45.2 Hz, 2H), 3.66–3.48 (m, 1H), 3.36 (dd, *J* = 4.8, 13.8 Hz, 1H), 3.09 (dd, *J* = 9.4, 13.5 Hz, 1H). ¹³C NMR (100 MHz, CD₃OD) δ (ppm): 175.99, 170.18, 165.00 (d, *J*_{CF} = 19.3 Hz), 140.78, 135.25, 133.15, 132.56, 129.74, 128.55, 126.66, 79.31 (d, *J*_{CF} = 176.6 Hz), 56.16, 38.93. HRMS (ESI) *m/z* calculated for [C₁₈H₂₀FN₄O₂⁺], 343.1570; observed, 343.1570.

***N*-Benzoyl-(*m*-nitro)phenylglycine (21).** To a solution of *m*-nitrophenylglycine⁴⁴ (500 mg, 2.55 mmol) and NaHCO₃ (715 mg, 675 mmol) in H₂O (13 mL) and 1,4-dioxane (2.8 mL) was added

benzoyl chloride (358 mg, 2.55 mmol in 1,4-dioxane (2.8 mL)), and the reaction was stirred at rt. After 2.5 h, the reaction was diluted with H₂O (80 mL), acidified with concentrated HCl (pH ~1.0), and extracted with ether (3 × 100 mL). The organics were combined, washed with brine (10 mL), dried over MgSO₄, and concentrated under reduced pressure. The remaining residue crystallized upon the addition of ether, and the product was collected by filtration as a white powder (575 mg, 75%). ¹H NMR (300 MHz, CD₃OD) δ (ppm): 8.42 (m, 1H), 8.27–8.18 (m, 1H), 7.95–7.85 (m, 3H), 7.67–7.41 (m, 4H), 5.87 (s, 1H). ¹³C NMR (75 MHz, CD₃OD) δ (ppm): 171.14, 168.48, 139.38, 134.00, 133.46, 131.68, 129.52, 128.74, 128.20, 127.24, 123.29, 122.68, 122.39. HRMS (ESI) *m/z* calculated for [C₁₅H₁₃N₂O₅⁺], 301.0824; observed, 301.0824.

N¹-Boc-N⁴-Benzoyl-1,4-diaminobutane (22). To a solution of N¹-Boc-1,4-diaminobutane·HCl (50 mg, 0.22 mmol) and Na₂CO₃ (70 mg, 0.66 mmol) in a mixture of H₂O (1 mL) and 1,4-dioxane (0.25 mL) was added benzoyl chloride (0.027 mL, 0.23 mmol). After stirring overnight at rt, the reaction mixture was partitioned between ether (10 mL) and 1 M HCl (5 mL). The organic layer was subsequently separated and washed with 5 mL portions of 1 M HCl, H₂O, and brine, dried over MgSO₄, and concentrated under reduced pressure to yield the title compound as a white solid (60.8 mg, 95%). ¹H NMR (400 MHz, CDCl₃) δ (ppm): 7.73 (d, *J* = 7.2 Hz, 2H), 7.40 (m, 1H), 7.33 (m, 2H), 6.69 (br, 1H), 4.71 (br, 1H), 3.39 (q, *J* = 6.4 Hz, 2H), 3.07 (q, *J* = 6.4 Hz, 2H), 1.61–1.45 (m, 4H), 1.36 (s, 9H). ¹³C NMR (75 MHz, CDCl₃) δ (ppm): 167.65, 156.24, 134.60, 131.32, 128.46, 126.97, 79.21, 39.62, 28.39, 27.67, 26.58. HRMS (ESI) *m/z* calculated for [C₁₆H₂₅N₂O₃⁺], 293.1865; observed, 293.1860.

N¹-Benzoyl-1,4-diaminobutane·TFA (23). Cold TFA (3 mL) was added to a reaction vial containing N¹-Boc-N⁴-benzoyl-1,4-diaminobutane (46.4 mg, 0.16 mmol), and the mixture was stirred at 0 °C. After 30 min, the reaction was allowed to warm to rt and was stirred for an additional 30 min before the excess TFA was removed. The resulting residue was dissolved in H₂O (6 mL), washed with ether (3 mL), and lyophilized to yield the title compound as a clear colorless residue (47.9 mg, 98%). ¹H NMR (400 MHz, D₂O) δ (ppm): 7.58 (m, 2H), 7.42 (m, 1H), 7.35 (m, 2H), 3.21 (t, *J* = 6.4 Hz, 2H), 2.85 (t, *J* = 7.0 Hz, 2H), 1.58 (m, 4H). ¹³C NMR (75 MHz, D₂O) δ (ppm): 170.82, 133.47, 131.96, 128.63, 126.83, 38.99, 25.43, 24.11. HRMS (ESI) *m/z* calculated for [C₁₁H₁₇N₂O⁺], 193.1341; observed, 193.1335.

N¹-Boc-N⁴-Benzenesulfonyl-1,4-diaminobutane (24). To a solution of N¹-Boc-1,4-diaminobutane·HCl (50 mg, 0.22 mmol) and Na₂CO₃ (70 mg, 0.66 mmol) in a mixture of H₂O (1 mL) and 1,4-dioxane (0.25 mL) was added benzenesulfonyl chloride (0.029 mL, 0.23 mmol) in 1,4-dioxane (0.25 mL). After stirring overnight at rt, the reaction mixture was partitioned between ether (10 mL) and 1 M HCl (5 mL). The organic layer was subsequently separated and washed with 5 mL portions of 1 M HCl, H₂O, and brine, dried over MgSO₄, and concentrated under reduced pressure to yield the title compound as a clear colorless residue (61.5 mg, 85%). ¹H NMR (400 MHz, CDCl₃) δ (ppm): 7.85 (m, 2H), 7.51 (m, 1H), 7.45 (m, 2H), 5.33 (br, 1H), 4.58 (br, 1H), 2.95 (m, 2H), 2.85 (q, *J* = 6.4 Hz, 2H), 1.41 (m, 4H), 1.38 (s, 9H). ¹³C NMR (75 MHz, CDCl₃) δ (ppm): 156.10, 139.91, 132.56, 129.09, 127.20, 126.98, 79.20, 42.80, 39.86, 28.38, 27.10, 26.66. HRMS (ESI) *m/z* calculated for [C₁₅H₂₅N₂O₄S⁺], 329.1535; observed, 329.1532.

N¹-Benzenesulfonyl-1,4-diaminobutane·TFA (25). Cold TFA (3 mL) was added to a reaction vial containing N¹-Boc-N⁴-sulfonyl-1,4-diaminobutane (54.5 mg, 0.17 mmol), and the mixture was stirred at 0 °C. After 30 min, the reaction was allowed to warm to rt and was stirred for an additional 30 min before the excess TFA was removed. The resulting residue was dissolved in H₂O (6 mL), washed with ether (3 mL), and lyophilized to yield the title compound as a clear colorless residue (50.9 mg, 87%). ¹H NMR (400 MHz, D₂O) δ (ppm): 7.69 (m, 2H), 7.54 (m, 1H),

7.43 (m, 2H), 2.79 (m, 4H), 1.49 (m, 2H), 1.35 (m, 2H). ^{13}C NMR (75 MHz, D_2O) δ (ppm): 137.88, 133.44, 129.44, 126.51, 41.87, 38.83, 25.56, 23.80. HRMS (ESI) m/z calculated for $[\text{C}_{10}\text{H}_{17}\text{N}_2\text{O}_2\text{S}^+]$, 229.1010; observed, 229.1010.

N^1 -(2-Hydroxy-5-nitro)benzoyl-L-ornithine·TFA (26). Rink AM Amide resin (300 mg, 0.2 mmol) was treated twice with 5 mL of 20% piperidine (in DMF) for 20 min and subsequently washed with dry DMF (3×5 mL). Fmoc-Orn(Boc)-OH (364 mg, 0.8 mmol), HBTU (303 mg, 0.8 mmol), HOBt (122 mg, 0.8 mmol), and triethylamine (0.22 mL, 1.6 mmol) were dissolved in dry DMF (5 mL) and allowed to react for 10 min before being added to the resin. The reaction mixture was rocked at rt for 3 h before the resin was filtered, washed with DMF (3×5 mL), treated twice with 5 mL of 20% piperidine (in DMF), and washed with dry DMF (3×5 mL). 5-Nitrosalicylic acid (147 mg, 0.8 mmol), HBTU (303 mg, 0.8 mol), HOBt (122 mg, 0.8 mmol), and triethylamine (0.22 mL, 1.6 mmol) were dissolved in dry DMF (5 mL) and allowed to react for 10 min before being added to the resin. The reaction mixture was rocked at rt for 6 h. The resin was filtered and washed with DMF (3×5 mL), ethanol (3×5 mL), and DCM (5 mL). The resin was dried under reduced pressure for 1 h prior to being treated three times with 5 mL of TFA/TIS/ H_2O (95/2.5/2.5) for 1 h. The filtrates were collected, combined, and concentrated prior to the addition of ether (25 mL). The resulting precipitate was collected by centrifugation and washed with an additional portion of ether. The crude product was purified by RP-HPLC to yield the title compound as a yellow powder (15.1 mg, 18%). ^1H NMR (400 MHz, CD_3OD) δ (ppm): 8.89 (d, $J = 2.8$ Hz, 1H), 8.29 (dd, $J = 2.4, 9.2$ Hz, 1H), 7.09 (d, $J = 9.2$ Hz, 1H), 4.70 (dd, $J = 5.2, 8.4$ Hz, 1H), 2.98 (m, 2H), 2.09 (m, 1H), 1.91 (m, 1H), 1.78 (m, 2H). ^{13}C NMR (100 MHz, CD_3OD) δ (ppm): 174.37, 166.60, 163.98, 140.16, 128.39, 125.47, 117.64, 116.61, 52.45, 38.84, 28.97, 23.59. HRMS (ESI) m/z calculated for $[\text{C}_{12}\text{H}_{17}\text{N}_4\text{O}_5^+]$, 297.1199; observed, 297.1207.

N^1 -(3-Carbonyl)pyrrole-L-ornithine Amide·TFA (27). Rink AM Amide resin (300 mg, 0.2 mmol) was treated twice with 5 mL of 20% piperidine (in DMF) for 20 min and subsequently washed with dry DMF (3×5 mL). Fmoc-Orn(Boc)-OH (364 mg, 0.8 mmol), HBTU (303 mg, 0.8 mmol), HOBt (122 mg, 0.8 mmol), and triethylamine (0.22 mL, 1.6 mmol) were dissolved in dry DMF (5 mL) and allowed to react for 10 min before being added to the resin. The reaction mixture was rocked at rt for 3 h before the resin was filtered, washed with DMF (3×5 mL), treated twice with 5 mL of 20% piperidine (in DMF), and washed with dry DMF (3×5 mL). 1H-Pyrrole-3-carboxylic acid (89 mg, 0.8 mmol), HBTU (303 mg, 0.8 mol), HOBt (122 mg, 0.8 mmol), and triethylamine (0.22 mL, 1.6 mmol) were dissolved in dry DMF (5 mL) and allowed to react for 10 min before being added to the resin. The reaction mixture was rocked at rt for 6 h. The resin was filtered and washed with DMF (3×5 mL), ethanol (3×5 mL), and DCM (5 mL). The resin was dried under reduced pressure for 1 h prior to being treated three times with 5 mL of TFA/TIS/ H_2O (95/2.5/2.5) for 1 h. The filtrates were collected, combined, and concentrated prior to the addition of ether (25 mL). The resulting precipitate was collected by centrifugation and washed with an additional portion of ether. The crude product was purified by RP-HPLC to yield the title compound as an off-white solid (19.5 mg, 29%). ^1H NMR (400 MHz, D_2O) δ (ppm): 10.7 (br, 1H), 6.91 (s, 1H), 6.75 (s, 1H), 6.11 (s, 1H), 4.27 (dd, $J = 5.2, 9.2$ Hz, 1H), 2.85 (t, $J = 7.2$ Hz, 2H), 1.91–1.51 (m, 4H). ^{13}C NMR (100 MHz, D_2O) δ (ppm): 176.70, 175.37, 123.94, 123.38, 112.04, 109.60, 52.81, 38.71, 27.80, 23.37. HRMS (ESI) m/z calculated for $[\text{C}_{10}\text{H}_{17}\text{N}_2\text{O}_2^+]$, 225.1351; observed, 225.1346.

N^1 -(2-Carboxy)benzoyl- N^5 -Boc-L-ornithine Amide·TFA (28). To a solution of H-Orn(Boc)-OH (232 mg, 1.0 mmol) and triethylamine (0.14 mL, 1.0 mmol) in H_2O (1 mL) was added phthalic anhydride (148 mg, 1.0 mmol, dissolved in 3 mL of THF). A second portion of triethylamine (0.14 mL, 1.0 mmol) was added, and the reaction was stirred

at rt for 2 h. The THF was removed under reduced pressure, and the remaining solution was acidified with concentrated HCl to pH \sim 1. (Note: Acidification results in the precipitation of a white solid.) The acidified mixture was extracted with DCM (3×3 mL). The organics were combined, washed with H_2O (2×2 mL) and brine (2 mL), dried over MgSO_4 , and concentrated to afford the title compound as a white powder (300 mg, 79%). ^1H NMR (300 MHz, CD_3OD) δ (ppm): 7.95 (m, 1H), 7.65–7.45 (m, 3H), 4.59 (m, 1H), 3.12 (m, 2H), 2.05–1.55 (m, 4H), 1.4 (s, 9H). ^{13}C NMR (75 MHz, CD_3OD) δ (ppm): 173.96, 171.29, 167.97, 157.20, 131.64, 130.66, 129.84, 129.60, 129.24, 127.60, 78.58, 52.51, 39.48, 28.43, 27.39, 25.88. HRMS (ESI) m/z calculated for $[\text{C}_{18}\text{H}_{25}\text{N}_2\text{O}_7^+]$, 381.1662; observed, 381.1668.

IC_{50} Values. IC_{50} values were measured as previously described.^{21,45,46} Briefly, PAD4 (0.2 μM) was preincubated with varying concentrations of inhibitor in Reaction Buffer (100 mM Tris-HCl pH 7.6, 10 mM CaCl_2 , 2 mM DTT, and 50 mM NaCl) for 15 min at 37 °C. BAEE (10 mM) was added, and the reaction was allowed to proceed for 15 min at 37 °C. The initial rate data were fit to eq 1 using GraFit 5.0.1.1.⁴⁷

$$\text{Fractional activity of PAD} = 1/(1 + [\text{I}]/\text{IC}_{50}) \quad (1)$$

Reversibility of Inhibition. To demonstrate that *o*-F- and *o*-Cl-amidine irreversibly inactivate all four PAD isozymes, PAD1 (2 μM), PAD2 (5 μM), PAD3 (5 μM), and PAD4 (2 μM) were treated with excess inhibitor (1 mM final) for 1 h. The reactions were then dialyzed for 20 h against a buffer (2 L) containing 20 mM Tris-HCl at pH 8.0, 1 mM EDTA, 2 mM DTT, 500 mM NaCl, and 10% glycerol. Residual activity was then measured using our standard citrulline production assay.^{2,48}

Substrate Protection. To demonstrate that the substrate protects against the inactivation by *o*-F- and *o*-Cl-amidine, reaction mixtures containing 100 mM Tris-HCl at pH 7.6, 2 mM DTT, 50 mM NaCl, 10 mM CaCl_2 , and 10 mM or 2 mM BAEE were preincubated with and without inactivator for 10 min. Enzymes (PAD1 (0.2 μM), PAD2 (0.5 μM), PAD3 (0.5 μM), or PAD4 (0.2 μM)) were added, and aliquots were removed at different time points (0–15 min for PAD1, PAD2, and PAD4 and 0–30 min for PAD3). The amount of product formed was measured as previously described,^{2,48} and the data were fit to eq 2 using GraFit (version 5.0.11),⁴⁷ where v_i is the initial velocity, $k_{\text{obs.app}}$ is the apparent pseudo-first order rate constant for inactivation, t is time, and P is the amount of product formed during the reaction.

$$P = v_i(1 - e^{-k_{\text{obs.app}}t})/k_{\text{obs.app}} \quad (2)$$

Inactivation Kinetics. The inactivation kinetic parameters were determined by incubating PAD1, 2, 3, or 4 in an inactivation mixture containing 10 mM CaCl_2 , 2 mM DTT, and 100 mM Tris-HCl at pH 7.6, and aliquots were taken out at different time points from 0 to 30 min. These aliquots were added to a reaction mixture containing 100 mM Tris-HCl pH at 7.6, 10 mM CaCl_2 , 2 mM DTT, 50 mM NaCl, and 10 mM BAEE. The reactions were quenched in liquid nitrogen after a 15 min incubation. The residual activity was then measured at each of the different concentrations of inactivator as a function of time, and the data were fit to eq 3 using GraFit version 5.0.11,⁴⁷ where v is the velocity, v_0 is the initial velocity, k is the pseudo-first order rate constant of inactivation (i.e., k_{obs}), and t is time.

$$v = v_0e^{-kt} \quad (3)$$

The k_{obs} values were then plotted versus inactivator concentration, and, for the case where saturation was achieved, the data were fit to eq 4 using GraFit version 5.0.11.⁴⁷ k_{inact} corresponds to the maximal rate of inactivation and K_i is the concentration of I that yields half-maximal inactivation.

$$k_{\text{obs}} = k_{\text{inact}}[\text{I}]/(K_i + [\text{I}]) \quad (4)$$

If saturation was not seen, and the plot of k_{obs} versus $[I]$ was linear, then the slope of the line corresponded to k_{inact}/K_I .

Cell Culture and Cytotoxicity Assay. HL60 human promyelocytic leukemia cells were cultured in RPMI 1640 media supplemented with 10% FBS and 1% penicillin–streptomycin. Cells were grown in a 5% CO₂ incubator at 37 °C. HL-60 cells were grown to a confluence of 1×10^6 cells/mL in the appropriate media. Ninety microliters of the cells were added to each well of a 96 well plate. *o*-F-amidine, *o*-Cl-amidine, or doxorubicin, (10 μ L; 100 nM to 100 μ M final) were added to the plates and allowed to incubate with the cells for 24 h. Cell viability was determined using the CellTiter 96 Nonradioactive Cell Proliferation Assay (Promega). Cell viability was quantified as the percentage of control absorbance. Each condition was performed in triplicate. The use of 1% Triton X-100 served as a 100% killing control. When possible, EC₅₀ values were determined by fitting the dose–response data to eq 1 using GraFit (version 5.0.11).⁴⁷ Here, $[I]$ is the concentration of inhibitor (e.g., doxorubicin), and EC₅₀ is the concentration of inhibitor that yields half-maximal cell survival.

Histone Deimination. HL60 cells (1×10^6 mL/cell) were treated with ATRA (1 μ M final concentration) for 48 h at 37 °C, 5% CO₂. Cells were split into 12 well plates and treated with 2 mM CaCl₂ and *o*-F-amidine, *o*-Cl-amidine, or Cl-amidine (1 μ M to 100 μ M). After 15 min at 37 °C in an atmosphere containing 5% CO₂, the calcium ionophore A23187 (4 μ M) was added. Cells were harvested after a 15 min treatment with the stimuli, rinsed with cold PBS, and lysed with SDS lysis buffer (2% SDS, 62.5 mM Tris, pH 6.8, 10% glycerol). Proteins were separated by SDS–PAGE and transferred to a nitrocellulose membrane for Western blot analysis. Membranes were blocked with 5% nonfat dried milk in TBST for 1 h at room temperature and subsequently probed with polyclonal anticitrulline H3 antibody (Abcam, ab5103) or polyclonal antiactin (Abcam, ab1801).

Cell Culture and Treatment. TK6 lymphoblastoid cells were a kind gift from Curtis C. Harris (National Cancer Institute, Bethesda, MD), originally derived from Dr. William Thilly's and Howard Liber's laboratories. TK6 cells are a lymphoblastoid cell line derived from the spleen more than 30 y ago. TK6 cells were maintained in an exponentially growing suspension culture at 37 °C in a humidified 5% CO₂ atmosphere in RPMI 1640 supplemented with 10% heat-inactivated calf serum, 100 units/mL penicillin, 100 μ g/mL streptomycin, and 2 mmol/L L-glutamine. Twelve hours before treatment, media were changed to that above, except supplemented with 1% heat-inactivated calf serum. Treatment was with 50 μ g/mL Cl-amidine or *o*-F-amidine for 0–24 h as indicated.

Apoptosis. Apoptosis was measured by Annexin V as previously described.²⁷ PARP cleavage was measured by standard Western blot procedures as described previously.⁴⁹ The antibodies were anti-PARP (Cell Signaling Technology, Cat#9542) and GAPDH (Abcam, ab9484).

Crystallization of PAD4 Inhibitor Complexes and Structure Determination. Crystals of *o*-F-amidine or *o*-Cl-amidine in complex with wild-type PAD4 were prepared by soaking the compound into crystals of wild-type PAD4. Crystals of the wild-type enzymes were prepared according to previously established methods.^{50,51} Subsequently, these crystals were transferred to fresh crystallization buffer containing 5 mM CaCl₂ and 5 mM *o*-F-amidine or *o*-Cl-amidine for 6 h. Diffraction data were then collected on a beamline BL-17A at Photon Factory (Tsukuba, Japan) and then scaled using the program HKL2000.⁵² The initial structure of the PAD4·*o*-F-amidine·calcium complex or PAD4·*o*-Cl-amidine·calcium complex was derived from the atomic coordinates of the PAD4(C645A)·BAA·calcium complex (Protein Data Bank entry: 1WDA). The structures were manually improved using the program COOT.⁵³ At this stage, the inhibitor moiety in the complex was identified on the $|F_o| - |F_c|$ electron density maps. The structures were refined by the programs CNS⁵⁴ and REFMAC.⁵⁵ Crystallographic data were given in Table 1. Final coordinates and structure factors have been

deposited to the Protein Data Bank Japan (PDBj). The PDB identification numbers are 1B1U and 1B1T for the PAD4·*o*-F-amidine and PAD4·*o*-Cl-amidine complexes, respectively.

■ ASSOCIATED CONTENT

S Supporting Information. The percent activity remaining after 20 h dialysis of the enzyme/inactivator complex and substrate protection experiments with *o*-F- and *o*-Cl-amidine. This material is available free of charge via the Internet at <http://pubs.acs.org>.

Accession Codes

[†]The coordinates for the PAD4·*o*-F-amidine and PAD4·*o*-Cl-amidine complexes have been deposited in the PDBJ. The PDB identification numbers are 1B1U and 1B1T, respectively.

■ AUTHOR INFORMATION

Corresponding Author

*Tel: (561)-228-2471. Fax: (561)-228-3050. E-mail: Pthompson@scripps.edu.

Author Contributions

⊗These authors contributed equally to this work.

■ ACKNOWLEDGMENT

This work was supported in part by funds from the University of South Carolina (to P.R.T.), The Scripps Research Institute, and by National Institutes of Health grants GM079357 (to P.R.T.) and CA151304 (to P.R.T. and L.J.H.).

■ ABBREVIATIONS USED

PAD, protein arginine deiminase; Cit, citrulline; RA, rheumatoid arthritis; BAEE, benzoyl-L-arginine ethyl ester; BAA, benzoyl-L-arginine amide; BAME, benzoyl-L-arginine methyl ester; DTT, dithiothreitol; TCEP, tris-2-carboxyethyl phosphine; EDTA, ethylenediaminetetraacetic acid; PTM, post-translational modification; NET, neutrophil extracellular trap; DSS, dextran sodium sulfate; HOTT, *S*-(1-oxido-2-pyridyl)-thio-*N,N,N,N'*-tetramethyluronium hexafluorophosphate; HBTU, 2-(1*H*-benzotriazol-1-yl)-1,1,3,3-tetramethyluronium hexafluorophosphate; TIS, triisopropyl silane

■ REFERENCES

- (1) Jones, J. E.; Causey, C. P.; Knuckley, B.; Slack-Noyes, J. L.; Thompson, P. R. Protein arginine deiminase 4 (PAD4): Current understanding and future therapeutic potential. *Curr. Opin. Drug Discovery Dev.* **2009**, *12*, 616–627.
- (2) Kearney, P. L.; Bhatia, M.; Jones, N. G.; Luo, Y.; Glascock, M. C.; Catchings, K. L.; Yamada, M.; Thompson, P. R. Kinetic characterization of protein arginine deiminase 4: a transcriptional corepressor implicated in the onset and progression of rheumatoid arthritis. *Biochemistry* **2005**, *44*, 10570–10582.
- (3) Vossenaar, E. R.; Zendman, A. J.; van Venrooij, W. J.; Pruijn, G. J. PAD, a growing family of citrullinating enzymes: genes, features and involvement in disease. *BioEssays* **2003**, *25*, 1106–1118.
- (4) Knuckley, B.; Causey, C. P.; Jones, J. E.; Bhatia, M.; Dreyton, C. J.; Osborne, T. C.; Takahara, H.; Thompson, P. R. Substrate specificity and kinetic studies of PADs 1, 3, and 4 identify potent and selective inhibitors of protein arginine deiminase 3. *Biochemistry* **2010**, *49*, 4852–63.

- (5) Raijmakers, R.; Zendman, A. J.; Egberts, W. V.; Vossenaar, E. R.; Raats, J.; Soede-Huijbregts, C.; Rutjes, F. P.; van Veen, P. A.; Drijfhout, J. W.; Puijn, G. J. Methylation of arginine residues interferes with citrullination by peptidylarginine deiminases in vitro. *J. Mol. Biol.* **2007**, *367*, 1118–1129.
- (6) Ishida-Yamamoto, A.; Senshu, T.; Takahashi, H.; Akiyama, K.; Nomura, K.; Iizuka, H. Decreased deiminated keratin K1 in psoriatic hyperproliferative epidermis. *J. Invest. Dermatol.* **2000**, *114*, 701–705.
- (7) Steinert, P. M.; Parry, D. A.; Marekov, L. N. Trichohyalin mechanically strengthens the hair follicle: multiple cross-bridging roles in the inner root sheath. *J. Biol. Chem.* **2003**, *278*, 41409–41419.
- (8) Lamensa, J. W.; Moscarello, M. A. Deimination of human myelin basic protein by a peptidylarginine deiminase from bovine brain. *J. Neurochem.* **1993**, *61*, 987–996.
- (9) Pritzker, L. B.; Joshi, S.; Gowan, J. J.; Harauz, G.; Moscarello, M. A. Deimination of myelin basic protein. I. Effect of deimination of arginyl residues of myelin basic protein on its structure and susceptibility to digestion by cathepsin D. *Biochemistry* **2000**, *39*, 5374–5381.
- (10) Wright, P. W.; Bolling, L. C.; Calvert, M. E.; Sarmiento, O. F.; Berkeley, E. V.; Shea, M. C.; Hao, Z.; Jayes, F. C.; Bush, L. A.; Shetty, J.; Shore, A. N.; Reddi, P. P.; Tung, K. S.; Samy, E.; Allietta, M. M.; Sherman, N. E.; Herr, J. C.; Coonrod, S. A. ePAD, an oocyte and early embryo-abundant peptidylarginine deiminase-like protein that localizes to egg cytoplasmic sheets. *Dev. Biol.* **2003**, *256*, 73–88.
- (11) Cuthbert, G. L.; Daujat, S.; Snowden, A. W.; Erdjument-Bromage, H.; Hagiwara, T.; Yamada, M.; Schneider, R.; Gregory, P. D.; Tempst, P.; Bannister, A. J.; Kouzarides, T. Histone deimination antagonizes arginine methylation. *Cell* **2004**, *118*, 545–553.
- (12) Wang, Y.; Wysocka, J.; Sayegh, J.; Lee, Y. H.; Perlin, J. R.; Leonelli, L.; Sonbuchner, L. S.; McDonald, C. H.; Cook, R. G.; Dou, Y.; Roeder, R. G.; Clarke, S.; Stallcup, M. R.; Allis, C. D.; Coonrod, S. A. Human PAD4 regulates histone arginine methylation levels via demethylation. *Science* **2004**, *306*, 279–283.
- (13) Li, P.; Yao, H.; Zhang, Z.; Li, M.; Luo, Y.; Thompson, P. R.; Gilmour, D. S.; Wang, Y. Regulation of p53 target gene expression by peptidylarginine deiminase 4. *Mol. Cell. Biol.* **2008**, *28*, 4745–4758.
- (14) Yao, H.; Li, P.; Venters, B. J.; Zheng, S.; Thompson, P. R.; Pugh, B. F.; Wang, Y. Histone Arg modifications and p53 regulate the expression of OKL38, a mediator of apoptosis. *J. Biol. Chem.* **2008**, *283*, 20060–20068.
- (15) Zhang, X.; Gamble, M. J.; Stadler, S.; Cherrington, B. D.; Causey, C. P.; Thompson, P. R.; Roberson, M. S.; Kraus, W. L.; Coonrod, S. A. Genome-wide analysis reveals PADI4 cooperates with Elk-1 to activate c-Fos expression in breast cancer cells. *PLoS Genet.* **2011**, *7*, e1002112.
- (16) Liu, G. Y.; Liao, Y. F.; Chang, W. H.; Liu, C. C.; Hsieh, M. C.; Hsu, P. C.; Tsay, G. J.; Hung, H. C. Overexpression of peptidylarginine deiminase IV features in apoptosis of haematopoietic cells. *Apoptosis* **2006**, *11*, 183–196.
- (17) Slack, J. L.; Causey, C. P.; Thompson, P. R. Protein arginine deiminase 4: a target for an epigenetic cancer therapy. *Cell. Mol. Life Sci.* **2011**, *68*, 709–720.
- (18) Loos, T.; Mortier, A.; Gouwy, M.; Ronsse, I.; Put, W.; Lenaerts, J. P.; Van Damme, J.; Proost, P. Citrullination of CXCL10 and CXCL11 by peptidylarginine deiminase: a naturally occurring posttranslational modification of chemokines and new dimension of immunoregulation. *Blood* **2008**, *112*, 2648–2656.
- (19) Proost, P.; Loos, T.; Mortier, A.; Schutyser, E.; Gouwy, M.; Noppen, S.; Dillen, C.; Ronsse, I.; Conings, R.; Struyf, S.; Opendakker, G.; Maudgal, P. C.; Van Damme, J. Citrullination of CXCL8 by peptidylarginine deiminase alters receptor usage, prevents proteolysis, and dampens tissue inflammation. *J. Exp. Med.* **2008**, *205*, 2085–2097.
- (20) Struyf, S.; Noppen, S.; Loos, T.; Mortier, A.; Gouwy, M.; Verbeke, H.; Huskens, D.; Luangsang, S.; Parmentier, M.; Geboes, K.; Schols, D.; Van Damme, J.; Proost, P. Citrullination of CXCL12 differentially reduces CXCR4 and CXCR7 binding with loss of inflammatory and anti-HIV-1 activity via CXCR4. *J. Immunol.* **2009**, *182*, 666–674.
- (21) Luo, Y.; Arita, K.; Bhatia, M.; Knuckley, B.; Lee, Y. H.; Stallcup, M. R.; Sato, M.; Thompson, P. R. Inhibitors and inactivators of protein arginine deiminase 4: functional and structural characterization. *Biochemistry* **2006**, *45*, 11727–11736.
- (22) Wang, Y.; Li, M.; Stadler, S.; Correll, S.; Li, P.; Wang, D.; Hayama, R.; Leonelli, L.; Han, H.; Grigoryev, S. A.; Allis, C. D.; Coonrod, S. A. Histone hypercitrullination mediates chromatin decondensation and neutrophil extracellular trap formation. *J. Cell Biol.* **2009**, *184*, 205–213.
- (23) Li, P.; Li, M.; Lindberg, M. R.; Kennett, M. J.; Xiong, N.; Wang, Y. PAD4 is essential for antibacterial innate immunity mediated by neutrophil extracellular traps. *J. Exp. Med.* **2010**, *207*, 1853–1862.
- (24) Neeli, I.; Khan, S. N.; Radic, M. Histone deimination as a response to inflammatory stimuli in neutrophils. *J. Immunol.* **2008**, *180*, 1895–1902.
- (25) Marcos, V.; Zhou, Z.; Yildirim, A. O.; Bohla, A.; Hector, A.; Vitkov, L.; Wiedenbauer, E. M.; Krautgartner, W. D.; Stoiber, W.; Belohradsky, B. H.; Rieber, N.; Kormann, M.; Koller, B.; Roscher, A.; Roos, D.; Griese, M.; Eickelberg, O.; Doring, G.; Mall, M. A.; Hartl, D. CXCR2 mediates NADPH oxidase-independent neutrophil extracellular trap formation in cystic fibrosis airway inflammation. *Nat. Med.* **2010**, *16*, 1018–1023.
- (26) Willis, V. C.; Gizinski, A. M.; Banda, N. K.; Causey, C. P.; Knuckley, B.; Cordova, K. N.; Luo, Y.; Levitt, B.; Glogowska, M.; Chandra, P.; Kulik, L.; Robinson, W. H.; Arend, W. P.; Thompson, P. R.; Holers, V. M. N- α -Benzoyl-N5-(2-chloro-1-iminoethyl)-L-ornithine amide, a protein arginine deiminase inhibitor, reduces the severity of murine collagen-induced arthritis. *J. Immunol.* **2011**, *186*, 4396–4404.
- (27) Chumanevich, A. A.; Causey, C. P.; Knuckley, B. A.; Jones, J. E.; Poudyal, D.; Chumanevich, A. P.; Davis, T.; Matesic, L. E.; Thompson, P. R.; Hofseth, L. J. Suppression of colitis in mice by Cl-amidine: a novel peptidylarginine deiminase (pad) inhibitor. *Am. J. Physiol.: Gastrointest. Liver Physiol.* **2011**, *300*, G929–G938.
- (28) Foulquier, C.; Sebbag, M.; Clavel, C.; Chapuy-Regaud, S.; Al Badine, R.; Mechin, M. C.; Vincent, C.; Nachat, R.; Yamada, M.; Takahara, H.; Simon, M.; Guerrin, M.; Serre, G. Peptidyl arginine deiminase type 2 (PAD-2) and PAD-4 but not PAD-1, PAD-3, and PAD-6 are expressed in rheumatoid arthritis synovium in close association with tissue inflammation. *Arthritis Rheum.* **2007**, *56*, 3541–3553.
- (29) Wood, D. D.; Ackerley, C. A.; Brand, B.; Zhang, L.; Raijmakers, R.; Mastronardi, F. G.; Moscarello, M. A. Myelin localization of peptidylarginine deiminases 2 and 4: comparison of PAD2 and PAD4 activities. *Lab. Invest.* **2008**, *88*, 354–364.
- (30) Schellekens, G. A.; de Jong, B. A.; van den Hoogen, F. H.; van de Putte, L. B.; van Venrooij, W. J. Citrulline is an essential constituent of antigenic determinants recognized by rheumatoid arthritis-specific autoantibodies. *J. Clin. Invest.* **1998**, *101*, 273–281.
- (31) Schellekens, G. A.; Visser, H.; de Jong, B. A.; van den Hoogen, F. H.; Hazes, J. M.; Breedveld, F. C.; van Venrooij, W. J. The diagnostic properties of rheumatoid arthritis antibodies recognizing a cyclic citrullinated peptide. *Arthritis Rheum.* **2000**, *43*, 155–163.
- (32) Harris, M. L.; Darrah, E.; Lam, G. K.; Bartlett, S. J.; Giles, J. T.; Grant, A. V.; Gao, P.; Scott, W. W., Jr.; El-Gabalawy, H.; Casciola-Rosen, L.; Barnes, K. C.; Bathon, J. M.; Rosen, A. Association of autoimmunity to peptidyl arginine deiminase type 4 with genotype and disease severity in rheumatoid arthritis. *Arthritis Rheum.* **2008**, *58*, 1958–1967.
- (33) Kolfenbach, J. R.; Deane, K. D.; Derber, L. A.; O'Donnell, C. I.; Gilliland, W. R.; Edison, J. D.; Rosen, A.; Darrah, E.; Norris, J. M.; Holers, V. M. Autoimmunity to peptidyl arginine deiminase type 4 precedes clinical onset of rheumatoid arthritis. *Arthritis Rheum.* **2010**, *62*, 2633–2639.
- (34) Suzuki, A.; Yamada, R.; Chang, X.; Tokuhira, S.; Sawada, T.; Suzuki, M.; Nagasaki, M.; Nakayama-Hamada, M.; Kawaida, R.; Ono, M.; Ohtsuki, M.; Furukawa, H.; Yoshino, S.; Yukioka, M.; Tohma, S.; Matsubara, T.; Wakitani, S.; Teshima, R.; Nishioka, Y.; Sekine, A.; Iida, A.; Takahashi, A.; Tsunoda, T.; Nakamura, Y.; Yamamoto, K. Functional haplotypes of PADI4, encoding citrullinating enzyme peptidylarginine

deiminase 4, are associated with rheumatoid arthritis. *Nat. Genet.* **2003**, *34*, 395–402.

(35) Iwamoto, T.; Ikari, K.; Nakamura, T.; Kuwahara, M.; Toyama, Y.; Tomatsu, T.; Momohara, S.; Kamatani, N. Association between PADI4 and rheumatoid arthritis: a meta-analysis. *Rheumatology* **2006**, *45*, 804–807.

(36) Lundberg, K.; Nijenhuis, S.; Vossenaar, E. R.; Palmblad, K.; van Venrooij, W. J.; Klareskog, L.; Zendman, A. J.; Harris, H. E. Citrullinated proteins have increased immunogenicity and arthritogenicity and their presence in arthritic joints correlates with disease severity. *Arthritis Res. Ther.* **2005**, *7*, R458–R467.

(37) Nakashima, K.; Hagiwara, T.; Ishigami, A.; Nagata, S.; Asaga, H.; Kuramoto, M.; Senshu, T.; Yamada, M. Molecular characterization of peptidylarginine deiminase in HL-60 cells induced by retinoic acid and 1 α ,25-dihydroxyvitamin D(3). *J. Biol. Chem.* **1999**, *274*, 27786–27792.

(38) Dong, S.; Zhang, Z.; Takahara, H. Estrogen-enhanced peptidylarginine deiminase type IV gene (PADI4) expression in MCF-7 cells is mediated by estrogen receptor- α -promoted transactivator protein-1, nuclear factor- κ B, and Sp1. *Mol. Endocrinol.* **2007**, *21*, 1617–1629.

(39) Valeriote, F.; Lin, H. Synergistic interaction of anticancer agents: a cellular perspective. *Cancer Chemother. Rep.* **1975**, *59*, 895–900.

(40) Jonsson, E.; Fridborg, H.; Nygren, P.; Larsson, R. Synergistic interactions of combinations of topotecan with standard drugs in primary cultures of human tumor cells from patients. *Eur. J. Clin. Pharmacol.* **1998**, *54*, 509–514.

(41) Causey, C. P.; Thompson, P. R. An improved synthesis of haloacetamide-based inactivators of protein arginine deiminase 4 (PAD4). *Tetrahedron Lett.* **2008**, *49*, 4383–4385.

(42) Knuckley, B.; Causey, C. P.; Pellechia, P. J.; Cook, P. F.; Thompson, P. R. Haloacetamide-based inactivators of protein arginine deiminase 4 (PAD4): evidence that general acid catalysis promotes efficient inactivation. *ChemBioChem* **2010**, *11*, 161–165.

(43) Knuckley, B.; Bhatia, M.; Thompson, P. R. Protein arginine deiminase 4: evidence for a reverse protonation mechanism. *Biochemistry* **2007**, *46*, 6578–6587.

(44) Sassatelli, M.; Debiton, E.; Aboab, B.; Prudhomme, M.; Moreau, P. Synthesis and antiproliferative activities of indolin-2-one derivatives bearing amino acid moieties. *Eur. J. Med. Chem.* **2006**, *41*, 709–716.

(45) Luo, Y.; Knuckley, B.; Bhatia, M.; Thompson, P. R. Activity based protein profiling reagents for protein arginine deiminase 4 (PAD4): synthesis and in vitro evaluation of a fluorescently-labeled probe. *J. Am. Chem. Soc.* **2006**, *128*, 14468–14469.

(46) Luo, Y.; Knuckley, B.; Lee, Y. H.; Stallcup, M. R.; Thompson, P. R. A fluoro-acetamide based inactivator of protein arginine deiminase 4 (PAD4): design, synthesis, and in vitro and in vivo evaluation. *J. Am. Chem. Soc.* **2006**, *128*, 1092–1093.

(47) Leatherbarrow, R. J. *GraFit*, version 5.0; Erathicus Software: Staines, UK, 2004.

(48) Knipp, M.; Vasak, M. A colorimetric 96-well microtiter plate assay for the determination of enzymatically formed citrulline. *Anal. Biochem.* **2000**, *286*, 257–264.

(49) Ying, L.; Marino, J.; Hussain, S. P.; Khan, M. A.; You, S.; Hofseth, A. B.; Trivers, G. E.; Dixon, D. A.; Harris, C. C.; Hofseth, L. J. Chronic inflammation promotes retinoblastoma protein hyperphosphorylation and E2F1 activation. *Cancer Res.* **2005**, *65*, 9132–9136.

(50) Arita, K.; Hashimoto, H.; Shimizu, T.; Yamada, M.; Sato, M. Crystallization and preliminary X-ray crystallographic analysis of human peptidylarginine deiminase V. *Acta Crystallogr., Sect. D: Biol. Crystallogr.* **2003**, *59*, 2332–2333.

(51) Arita, K.; Hashimoto, H.; Shimizu, T.; Nakashima, K.; Yamada, M.; Sato, M. Structural basis for Ca(2+)-induced activation of human PAD4. *Nat. Struct. Mol. Biol.* **2004**, *11*, 777–783.

(52) Otwinowski, Z.; Minor, W. Processing of X-ray diffraction data collected in oscillation mode. *Methods Enzymol.* **1997**, *276*, 307–326.

(53) Emsley, P.; Cowtan, K. Coot: model-building tools for molecular graphics. *Acta Crystallogr., Sect. D: Biol. Crystallogr.* **2004**, *60*, 2126–2132.

(54) Brunger, A. T.; Adams, P. D.; Clore, G. M.; DeLano, W. L.; Gros, P.; Grosse-Kunstleve, R. W.; Jiang, J. S.; Kuszewski, J.; Nilges, M.; Pannu, N. S.; Read, R. J.; Rice, L. M.; Simonson, T.; Warren, G. L. Crystallography & NMR system: A new software suite for macromolecular structure determination. *Acta Crystallogr., Sect. D: Biol. Crystallogr.* **1998**, *54*, 905–921.

(55) Murshudov, G. N.; Vagin, A. A.; Dodson, E. J. Refinement of macromolecular structures by the maximum-likelihood method. *Acta Crystallogr., Sect. D: Biol. Crystallogr.* **1997**, *53*, 240–255.